

1 **Functional SARS-CoV-2-specific immune memory persists after mild COVID-19**

2

3 **Authors:**

4 Lauren B. Rodda^{1,6}, Jason Netland^{1,6}, Laila Shehata^{1,7}, Kurt B. Pruner^{1,7}, Peter A. Morawski^{2,7},
5 Chris Thouvenel³, Kennedy K. Takehara¹, Julie Eggenberger⁴, Emily A. Hemann⁴, Hayley R.
6 Waterman², Mitchell L. Fahning², Yu Chen³, Jennifer Rathe⁴, Caleb Stokes⁴, Samuel Wrenn⁵,
7 Brooke Fiala⁵, Lauren Carter⁵, Jessica A. Hamerman^{1,2}, Neil P. King⁵, Michael Gale Jr⁴, Daniel
8 J. Campbell^{1,2}, David Rawlings^{1,3}, Marion Pepper^{1,8}

9

10 **Addresses:**

11 ¹Department of Immunology, University of Washington School of Medicine, Seattle, WA, USA.

12 ²Center for Fundamental Immunology, Benaroya Research Institute, Seattle, WA, USA.

13 ³Department of Pediatrics, University of Washington School of Medicine, Seattle, WA and
14 Center for Immunity and Immunotherapies, Seattle Children's Research Institute, Seattle, WA,
15 USA.

16 ⁴Department of Immunology, Center for Innate Immunity and Immune Disease, University of
17 Washington, Seattle, WA, USA.

18 ⁵Department of Biochemistry, University of Washington, Seattle, WA, USA and Institute for
19 Protein Design, University of Washington, Seattle, WA, USA.

20 ⁶These authors contributed equally.

21 ⁷These authors contributed equally.

22 ⁸email: mpepper@uw.edu

23

24 **Summary:**

25

26 **The recently emerged SARS-CoV-2 virus is currently causing a global pandemic and cases**
27 **continue to rise. The majority of infected individuals experience mildly symptomatic**
28 **coronavirus disease 2019 (COVID-19), but it is unknown whether this can induce persistent**
29 **immune memory that might contribute to herd immunity. Thus, we performed a**
30 **longitudinal assessment of individuals recovered from mildly symptomatic COVID-19 to**
31 **determine if they develop and sustain immunological memory against the virus. We found**
32 **that recovered individuals developed SARS-CoV-2-specific IgG antibody and neutralizing**
33 **plasma, as well as virus-specific memory B and T cells that not only persisted, but in some**
34 **cases increased numerically over three months following symptom onset. Furthermore, the**
35 **SARS-CoV-2-specific memory lymphocytes exhibited characteristics associated with potent**
36 **antiviral immunity: memory T cells secreted IFN- γ and expanded upon antigen re-**
37 **encounter, while memory B cells expressed receptors capable of neutralizing virus when**
38 **expressed as antibodies. These findings demonstrate that mild COVID-19 elicits memory**
39 **lymphocytes that persist and display functional hallmarks associated with antiviral**
40 **protective immunity.**

41

42 **Main Text:**

43

44 The rapid spread of the SARS-CoV-2 beta coronavirus has infected 19 million and killed over
45 700,000 people worldwide as of early August 2020. Infection causes the disease COVID-19, which
46 ranges in presentation from asymptomatic to fatal. However, the vast majority of infected

47 individuals experience mild symptoms that do not require hospitalization¹. It is critically important
48 to understand if SARS-CoV-2–infected individuals who recover from mild disease develop
49 immune memory that protects them from subsequent SARS-CoV-2 infections, thereby reducing
50 transmission and promoting herd immunity.

51
52 Immunological memory is predominantly mediated by cells of the adaptive immune system. In
53 response to most acute viral infections, B and T cells that can bind viral antigens through their
54 antigen receptors become activated, expand, differentiate and begin secreting effector molecules
55 to help control the infection. Upon resolution of infection, approximately 90% of these virus-
56 specific “effector cells” die, while 10% persist as long-lived “memory” cells². Immune memory
57 cells can produce a continuous supply of effector molecules, as seen with long-lived antibody-
58 secreting plasma cells (LLPCs). In most cases, however, quiescent memory lymphocytes are
59 strategically positioned to rapidly reactivate in response to re-infection and execute effector
60 programs imprinted upon them during the primary response. Upon re-infection, pathogen-specific
61 memory B cells (MBCs) that express receptors associated with antigen experience and the
62 transcription factor T-bet rapidly proliferate and differentiate into IgG⁺ antibody-secreting
63 plasmablasts (PBs)³⁻⁵. Reactivated T-bet–expressing memory CD4⁺ T cells proliferate, “help”
64 activate MBCs and secrete cytokines (including IFN γ) to activate innate cells². Meanwhile,
65 memory CD8⁺ T cells can kill virus-infected cells directly through the delivery of cytolytic
66 molecules⁶. These quantitatively and qualitatively enhanced virus-specific memory populations
67 coordinate to quickly clear the virus, thereby preventing disease and reducing the chance of
68 transmission.

69

70 To infect cells and propagate, SARS-CoV-2 relies on the interaction between the receptor binding
71 domain (RBD) of its spike protein (S) and angiotensin converting enzyme 2 (ACE2) on host cells⁷.
72 Multiple studies have shown that the majority of SARS-CoV-2 infected individuals produce S-
73 and RBD-specific antibodies during the primary response, and RBD-specific monoclonal
74 antibodies can neutralize the virus *in vitro* and *in vivo*⁸⁻¹⁰. Therefore, RBD-specific antibodies
75 would likely contribute to protection against re-infection if expressed by LLPCs or MBCs.

76
77 To determine if the above hallmarks of immune protection from viral infection both form and
78 persist in individuals that have experienced mild COVID-19, we assessed their SARS-CoV-2-
79 specific immune responses at one and three months post-symptom onset. Herein we demonstrate
80 that a multipotent SARS-CoV-2-specific immune memory response forms and is maintained in
81 recovered individuals at least for the duration of our study. Furthermore, memory lymphocytes
82 display hallmarks of protective antiviral immunity.

83
84 ***Return to immune homeostasis after mildly symptomatic COVID-19***

85
86 To determine if immune memory cells form after mildly symptomatic COVID-19, we collected
87 plasma and peripheral blood mononuclear cells (PBMCs) from 15 individuals recovered from
88 COVID-19 (CoV2⁺) (UW IRB 00009810). The CoV2⁺ group had a median age of 47 and reported
89 mild symptoms lasting a median of 13 days (**E.D. Table 1**). The first blood sample (Visit 1) was
90 drawn at least 20 days after a positive PCR test for SARS-CoV-2 and a median of 35.5 days post-
91 symptom onset. We expect the primary response to be contracting and early memory populations
92 to be generated at this time point, as viral load is cleared approximately 8 days post symptom onset

93 ¹¹. Participants returned for a second blood draw (Visit 2) a median of 86 days post-symptom onset
94 so we could assess the quantity and quality of the long-lived memory populations (**Fig. 1a**). We
95 compared these samples to samples collected at two time points representing a similar sampling
96 interval in a group of 17 healthy controls (HCs). All HCs were considered to have no prior SARS-
97 CoV-2 infection based on having no detectable plasma SARS-CoV-2 RBD- or S-specific
98 antibodies above three standard deviations (SDs) of the mean of historical negative (HN) plasma
99 samples (**E.D. Fig. 1**). We also included HN PBMC samples that were collected prior to the first
100 human SARS-CoV-2 infection (2016-2019). We included these to control for the possibility that
101 individuals in the HC group had been infected with SARS-CoV-2 (9/17 described having some
102 symptoms associated with SARS-CoV-2 infection) despite their lack of detectable RBD-specific
103 antibodies.

104
105 Populations of activated innate and adaptive immune cells expand in the blood during the primary
106 response to SARS-CoV-2 infection¹². When an acute viral infection is cleared, the majority of
107 these highly inflammatory cells either die or become quiescent memory cells such that the
108 proportions and phenotypes of total immune cells are indistinguishable from those seen in pre-
109 infection blood samples. Consistent with resolution of the primary response, we found no
110 differences in frequency of total monocytes, monocyte subsets or plasmacytoid dendritic cells
111 among PBMCs between CoV2⁺ and HC individuals (**E.D. Fig. 2**). We also found no differences
112 in $\gamma\delta$ or $\alpha\beta$ CD3⁺ T cell frequencies (CD4⁺ or CD8⁺), nor in the cell cycle status, expression of
113 molecules associated with activation, migration, function or proportions of various CD45RA⁻
114 memory T cell subsets (**E.D. Fig. 3**). Together, these data demonstrate that the inflammatory

115 response associated with acute infection had resolved by the Visit 1 time point and the early
116 immune memory phase had commenced.

117

118 *Mild COVID-19 induces persistent, neutralizing anti-SARS-CoV-2 IgG antibody*

119

120 Humoral immune responses are characterized by a first wave of short-lived, low-affinity antibody-
121 secreting PBs followed by a subsequent germinal center (GC) response that generates high-affinity
122 MBCs and antibody-secreting LLPCs. LLPCs can maintain detectable serum antibody titers for
123 months to many years, depending upon the specific viral infection¹³. Thus, it is critical to
124 distinguish the first wave of waning PB-derived antibodies from the later wave of persistent LLPC-
125 derived antibodies that can neutralize subsequent infections, potentially for life. We therefore first
126 determined that CD19⁺CD20^{lo}CD38^{hi} PBs were no longer present at elevated frequencies in
127 CoV2⁺ individuals relative to HCs at Visit 1 (**E.D. Fig. 4a**). Other measures of recent B cell
128 activation in non-PB B cells include increased Ki67 expression (indicating cells have entered the
129 cell cycle) and expression of T-bet¹⁴. There are small increases in both the frequencies of Ki67⁺
130 and T-bet⁺ B cells at the Visit 1 time point compared to HC, but not at the Visit 2 time point (**E.D.**
131 **Fig. 4b,c**). These data suggest that while PBs associated with controlling acute infection are no
132 longer detectable in CoV2⁺ individuals at Visit 1, other B cell fates are still contracting. However,
133 by Visit 2, these B cell phenotypes have returned to homeostasis (**E.D. Fig. 4a-c**).

134

135 Antibodies measured at Visit 1 might include contributions from short-lived plasmablasts, while
136 those measured at Visit 2, long after PBs have contracted, represent contributions from LLPCs in
137 the bone marrow. We therefore examined the SARS-CoV-2-specific IgG, IgM and IgA antibodies

138 at Visit 1 and Visit 2¹⁵. At Visit 1, 100% of CoV2⁺ individuals had plasma anti-RBD IgG levels 3
139 SDs above the mean of HCs, as measured by ELISA area under the curve (AUC), in accordance
140 with studies showing 100% seroprevalence by day 14¹⁰ (**Fig. 1b**). Additionally, 93% of CoV2⁺
141 individuals had anti-RBD IgM and 73% had anti-RBD IgA above this negative threshold. Almost
142 all CoV2⁺ individuals possessed IgG (100%), IgM (100%), and IgA (93%) anti-spike antibodies
143 above the threshold at Visit 1 as well (**E.D. Fig. 4d**). Levels of anti-RBD and anti-spike binding
144 were highly correlated for all isotypes (**E.D. Fig. 4e**). At Visit 2, all CoV2⁺ individuals maintained
145 anti-RBD IgG levels above the negative threshold and 71% and 36% had maintained anti-RBD
146 IgM and IgA, respectively (**Fig. 1b**). Anti-RBD IgG levels decreased only slightly among CoV2⁺
147 individuals between time points and 36% of CoV2⁺ individuals had the same or increased levels
148 at Visit 2. Anti-RBD IgM and IgA, however, decreased substantially from Visit 1 to Visit 2 (**Fig.**
149 **1c, E.D. Fig. 4f**).

150
151 As spike protein, and specifically the RBD, is key for viral entry into the cell, antibodies that target
152 the RBD can be potent inhibitors of infection^{8,9}. To determine whether CoV2⁺ individuals form
153 and maintain neutralizing antibodies, we tested for SARS-CoV-2 neutralization indirectly using a
154 cell-free competition assay (surrogate virus neutralization test, sVNT) and directly in a plaque
155 reduction neutralization test (PRNT)¹⁶. CoV2⁺ plasma inhibited RBD binding to ACE2
156 significantly more than HC plasma by sVNT and RBD inhibition correlated strongly with anti-
157 RBD IgG levels at both time points (**Fig. 1d,e**). Further, RBD inhibition capacity was maintained
158 or increased in the majority of CoV2⁺ individuals from Visit 1 to Visit 2 (**Fig. 1f, E.D. Fig. 4g**).
159 Neutralization by PRNT correlated strongly with RBD inhibition at both time points (**Fig. 1g, E.D.**
160 **4h**) and was similarly maintained between visits (**Fig. 1h**). By the latest time point in our study,

161 86% of CoV2⁺ individuals still had better RBD-inhibiting plasma than HCs and 71% had better
162 neutralizing plasma (measured as above HC mean + 3 SDs). These data are consistent with the
163 emergence of predominantly IgG⁺ RBD and spike-specific LLPCs that maintain detectable
164 neutralizing anti-SARS-CoV-2 antibody to at least 3 months post-symptom onset.

165

166 *Mild COVID-19 induces a sustained enrichment of RBD-specific memory B cells.*

167

168 The presence of SARS-CoV-2-neutralizing antibodies three months post-symptom onset in CoV2⁺
169 individuals suggests GC-derived memory LLPCs have formed. GC-derived MBCs also play a
170 critical role in the formation of antibody secreting cells upon antigen re-exposure. Therefore, we
171 tested whether SARS-CoV-2-specific MBCs were also formed and maintained in CoV2⁺
172 individuals throughout the study time course. We generated RBD tetramer reagents and used
173 enrichment strategies to identify rare RBD-specific cells that are otherwise undetectable in bulk
174 assessments¹⁷. We confirmed specificity in RBD immunized mice and then used the RBD-tetramer
175 to identify, enumerate and phenotype rare, RBD-specific B cells in our HN, HC and CoV2⁺
176 individuals (**E.D. Fig. 5a,b; Fig. 2a**). Gates used to phenotype RBD-specific B cells were defined
177 on total B cell populations (**E.D. Fig. 5c**). At Visit 1, RBD-specific B cells were significantly
178 expanded in CoV2⁺ individuals compared to HCs and their numbers were increased further at Visit
179 2 (**Fig. 2a, b**). The proportion and number of RBD-specific MBCs (defined by CD21 and CD27
180 expression) in CoV2⁺ samples was significantly greater than in HCs and increased from Visit 1 to
181 Visit 2 (**Fig. 2c,d, E.D. Fig. 5d**). While RBD-specific B cells in HN samples had a similar
182 proportion of MBCs as in CoV2⁺ samples, they contained substantially fewer cells. In addition,
183 RBD-specific MBCs were largely quiescent with very few expressing Ki67 (**Fig. 2e, E.D. Fig.**

184 switched B cell receptors (BCRs) is another marker of GC-derivation. We therefore assayed BCR
185 isotype expression on RBD-specific MBCs and found enriched populations of IgA- and IgG-
186 expressing MBCs in CoV2⁺ individuals at both time points (**Fig. 2f-h, E.D. Fig. 5f**). Of note, while
187 small numbers of RBD-specific MBCs were detected in controls, these cells were predominantly
188 unswitched (IgM⁺ and IgD⁺), suggesting they may represent cross-reactive MBCs possibly
189 generated in response to one of the human coronaviruses that cause 15% of common colds¹⁸⁻²⁰.

190
191 An additional measure of antiviral MBC function is the graded expression of T-bet¹⁴. MBCs that
192 express low-levels of T-bet are associated with rapid differentiation into secondary PBs that
193 produce high affinity, viral-specific antibodies during a secondary infection²¹. We found a higher
194 proportion and number of T-bet⁺, and specifically T-bet^{lo}, RBD-specific MBCs in CoV2⁺
195 individuals compared with HCs at Visit 1 and the higher numbers were maintained at Visit 2 (**Fig.**
196 **2i-k, E.D. Fig. 5g,h**). T-bet^{hi} MBCs are considered to be recently activated and often found
197 enriched during chronic infection²¹. Consistent with SARS-CoV-2 being an acute infection¹¹, we
198 found very few RBD-specific T-bet^{hi} MBCs in CoV2⁺ individuals at either memory time point
199 (**E.D. Fig. 5i**). Our data demonstrate that SARS-CoV-2 infection induces the generation of RBD-
200 specific Tbet^{lo}IgG⁺CD21⁺CD27⁺ “classical” MBCs likely derived from a GC²². Furthermore,
201 numbers of these MBCs were not only maintained, but increased from one to three months post-
202 symptom onset.

203

204 *SARS-CoV-2 infection induces durable, functional spike-reactive CD4⁺ T cells*

205

206 The presence of T-bet⁺ RBD-specific MBCs suggested that antigen-specific memory T cell
207 responses were also likely to be elicited in CoV2⁺ individuals. To enumerate SARS-CoV-2-
208 specific memory T cells, total PBMCs from control or CoV2⁺ individuals were incubated with
209 spike protein and expression of activation markers was assessed (**Fig. 3a**)^{23,24}. PBMCs from CoV2⁺
210 individuals at Visit 1 and 2 displayed robust re-activation of spike-specific CD4⁺ memory T
211 responses, as measured by increased expression of ICOS and CD40L (two molecules associated
212 with B cell help upon re-activation), while PBMCs from HC and HN individuals did not (**Fig.**
213 **3a,b**). There were no significant differences in the numbers of responding cells in CoV2⁺
214 individuals between the two visits, suggesting spike-specific memory CD4⁺ T cells were
215 maintained throughout the study (**Fig. 3b**). Furthermore, greater numbers of CXCR5-expressing
216 circulating T follicular helper (cTfh) cells²⁵, which provide B cell help, were found within the
217 population of S-specific ICOS⁺CD40L⁺CD4⁺ cells in CoV2⁺ individuals than in healthy controls
218 at both visits (**Fig. 3c**). Together these data suggest that SARS-CoV-2-specific memory CD4⁺ T
219 cells maintain the capacity to provide B cell help even at three months post-symptom onset.

220
221 Memory CD4⁺ T cells produce cytokines within hours of activation, whereas naive T cells take
222 days²⁶. We first examined cytokine production from activated CD4⁺ memory CXCR5⁻ non-Tfh
223 cells and CXCR5⁺ cTfh cells identified in the assay above (**Fig. 3b**). S-specific CCR6⁺CXCR5⁺
224 cTfh cells, associated with IL-17 production, and a smaller population of CXCR3⁺CXCR5⁺ cTfh
225 cells, associated with IFN γ production, were recently described in a predominantly mild to
226 moderate cohort 30 days post symptom onset²⁷. We therefore analyzed activated ICOS⁺CD69⁺ S-
227 specific cells for expression of CCR6 and CXCR5 and then cytokine expression was examined in
228 each population based on gating on a PMA positive control (**Fig 3d, E.F. 6a**). Although multiple

229 cytokines associated with Tfh function were assessed, only IFN γ , IL-17 and IL-2 cytokine
230 producing cells were significantly expressed in activated S-specific memory CD4⁺ cells in CoV2⁺
231 individuals compared to HCs (**Fig. 3d-f**). Small numbers of S-specific cells were measured in HCs
232 after stimulation compared to vehicle alone that reflect previously described S-specific cross-
233 reactivity^{20,28}, but far greater responses were seen in the CoV2⁺ individuals (**Fig. 3e**). Three months
234 post symptom onset we found a higher frequency of CCR6⁻ cTfh cells that produced Th1 cytokines,
235 IFN γ and IL-2, suggesting a dominant Th1 response in CoV2⁺ individuals (**Fig. 3f**).

236
237 To further define the types of antigen-specific CD4⁺ memory T cells in CoV2⁺ individuals without
238 relying on secretion of specific cytokines, we assessed memory CD4⁺ T cell proliferation in
239 response to spike restimulation. For this, we sorted CD45RA⁺ naive, CD45RA⁻CCR7⁺ central
240 memory (Tcm) and CD45RA⁻CCR7⁻ effector memory (Tem) T cells from HC or CoV2⁺
241 individuals (**E.D. Fig. 6b**), then measured the proliferative capacity of each sorted population
242 following culture with autologous CD14⁺ monocytes and recombinant spike protein (**Fig. 3g, h**;
243 **E.D. Fig 6c**). Only Tcm cells from CoV2⁺ individuals taken at both Visit 1 and Visit 2 displayed
244 significant proliferation frequencies compared to HC samples, although substantial proliferative
245 responses by Tem cells were observed in some CoV2⁺ individuals (**Fig. 3h**). We also examined
246 the expression of CXCR3 and CCR6 on S-specific, proliferated memory cells and found that the
247 majority of cells that had proliferated, as measured by the dilution of cell proliferation dye (CPD^{lo})
248 expressed CXCR3, in keeping with Type 1 cytokine production in the previous assay. Spike-
249 specific Tcm, and potentially Tem, are therefore maintained throughout our study and have the
250 ability to proliferate and re-populate the memory pool upon antigen re-encounter.

251

252 While much recent work has focused on antibodies and B cells, memory CD8⁺ T cells are uniquely
253 positioned to kill virus infected cells through their directed expression of cytokines and cytolytic
254 molecules. S-specific memory CD8⁺ T cells that persisted for three months after mild COVID-19
255 disease could be identified by expression of the activation marker CD69 and the cytokine IFN γ
256 after overnight stimulation with spike (**Fig 3i**). Unlike CD4⁺ memory T cells, activated cytokine-
257 expressing CD8⁺ T cells were significantly increased over vehicle controls in both control and
258 CoV2⁺ groups (**Fig. 3j**). Together, these data demonstrate that both CD4⁺ and CD8⁺ SARS-CoV-
259 2-specific memory T cells are maintained and are able to produce effector cytokines after
260 restimulation three months post-symptom onset in mildly symptomatic COVID-19 individuals.

261

262 *Mild COVID-19-induced SARS-CoV-2-specific MBCs can express neutralizing antibodies*

263

264 Since SARS-CoV-2 RBD-specific MBC and S-specific CD4⁺ cTfh were enriched in CoV2⁺
265 individuals after 3 months, we assessed whether these MBCs could produce neutralizing antibodies
266 if they were reactivated by a secondary infection. To this end, we index sorted single RBD-specific
267 B cells and sequenced the BCRs from 3 CoV2⁺ individuals at Visit 1 (**E.D. Fig. 7a**). Of the class-
268 switched (IgG⁺) RBD-specific classical MBCs (CD21⁺CD27⁺) we sorted, we randomly selected 7
269 to be cloned and expressed as IgG1 monoclonal antibodies (**Fig 4a**). This set of antibodies utilized
270 a wide variety of heavy and light chains, had all undergone somatic hypermutation and were all
271 unique clones (**Fig. 4b, E.D. Table 2**). These antibodies were first expressed in small scale
272 cultures. Transfection supernatants were assessed for antibody expression by IgG ELISA (**E.D.**
273 **Fig 7b**) and specificity by RBD ELISA where all 7 showed strong binding to RBD (**Fig. 4c**). The
274 first 4 antibodies cloned were expressed on a larger scale and purified. The specificity of these

275 purified antibodies for RBD was again confirmed by ELISA (**E.D. Fig. 7c**) and their ability to
276 prevent SARS-CoV-2 infection was tested via PRNT assay. Two of the four tested (#202 and 203)
277 showed strong virus neutralization (**Fig. 4d**), with IC₅₀ values of 15.6 and 15.4 ng/ml respectively
278 (**Fig. 4e**). This was comparable to a previously published strongly neutralizing mouse antibody
279 (B04) which was included as a positive control (IC₅₀= 3.6 ng/ml)²⁹. Two of the RBD-specific
280 antibodies were unable to inhibit virus infection, similar to a non-neutralizing mouse antibody
281 (C02) and an irrelevant *Plasmodium*-specific human antibody. Three more monoclonal antibodies
282 in addition to the 4 above were assessed for their capacity to inhibit RBD binding to the ACE2
283 receptor by sVNT assay (**Fig. 4f**). Three of the seven were able to inhibit RBD binding to ACE2,
284 similarly to a strongly neutralizing alpaca nanobody³⁰. Interestingly, #203, which neutralized live
285 virus, did not inhibit binding in this assay, while #202 both inhibited binding and neutralized the
286 virus. Overall 50% of the antibodies tested showed inhibitory activity by one or both of these
287 methods. Thus, RBD-specific MBCs induced by SARS-CoV-2 infection are capable of producing
288 neutralizing antibodies against the virus and could thus contribute to protection from a second
289 exposure to SARS-CoV-2.

290

291 ***Discussion***

292

293 In the absence of a vaccine, natural infection-induced herd immunity could play a key role in
294 reducing infections and deaths. For this to be possible, individuals that experience mild COVID-
295 19 would need to develop and sustain protective immune memory. Here, we found that individuals
296 that recovered from mildly symptomatic COVID-19 had an expanded arsenal of SARS-CoV-2-
297 specific immune mediators: neutralizing antibodies, IgG⁺T-bet^{lo} classical MBCs, circulating

298 cytokine-producing CXCR5⁺ Tfh1 cells, proliferating CXCR3⁺ CD4⁺ memory cells and IFN γ
299 producing CD8⁺ T cells that were maintained to at least three months post-symptom onset. This
300 study predicts that these recovered individuals will be protected from a second SARS-CoV-2
301 infection and, if so, suggests that Th1 memory should be the target of vaccine elicited memory.

302
303 Although long-lived immune memory can form to most viruses, some studies examining the
304 longevity of the response to coronaviruses have suggested that this is not the case³¹⁻³³. However,
305 more recent studies, including our own, have examined memory time points when only LLPCs,
306 and not short-lived PBs, are producing circulating antibodies. Our study, along with three others
307 clearly demonstrates elevated IgG⁺ RBD-specific plasma antibodies and neutralizing plasma are
308 generated and maintained for at least 3 months post-SARS-CoV-2 infection³⁴⁻³⁶.

309
310 While antibodies reveal the contributions of LLPCs, functional virus-specific memory B and T
311 cells can also be key to protective immune memory³⁷. Although previous studies have measured
312 the emergence of SARS-CoV-2-specific MBCs within a month of infection^{27,38}, we characterized
313 SARS-CoV-2-specific MBCs at one and three months from symptom onset. Our study revealed a
314 prominent population of RBD-specific IgG⁺CD27⁺CD21⁺T-bet^{lo} MBCs, which has been
315 associated in other infections with rapid differentiation into antibody-secreting PBs upon re-
316 exposure⁵, effective antiviral responses³⁹ and long-lived protection³. Furthermore, we found some
317 of the RBD-specific MBCs at Visit 1 expressed BCRs capable of neutralizing the virus when
318 expressed as antibodies. Since the numbers of these IgG⁺ RBD-specific MBCs were not only
319 sustained, but continued to increase between one and three months, we predict they are GC-
320 derived. Thus, MBCs at three months would have undergone increased affinity maturation and we

321 would expect an even higher percentage will be capable of producing neutralizing RBD-specific
322 antibodies upon re-infection.

323

324 MBC reactivation requires interactions with memory CD4⁺ T cells, which reactivate MBCs
325 through their expression of key molecules associated with T-B interactions including CXCR5,
326 ICOS, CD40 and a variety of cytokines. SARS-CoV-2-specific CD4⁺ memory T cells in recovered
327 individuals exhibited the capacity to express all of these molecules and to undergo robust
328 proliferation upon re-exposure to spike protein. Notably, S-specific CD4⁺ memory T cells from
329 CoV2⁺ individuals rapidly displayed increased levels of ICOS and CD40L on CXCR5⁺ and
330 CXCR5⁻ cells after stimulation as well as expression of Th1- and Th17- associated cytokines.
331 These results are consistent with another recent report of SARS-CoV-2- specific cTfh cells²⁷,
332 although they detected a high frequency of Th17-like cTfh cells, which could be due to the earlier
333 time point they were examining as Th17 cells can develop into Th1 cells late in an immune
334 response⁴⁰. The expression of IFN γ and IL-17 by these cells is notable as these cytokines are
335 associated with class-switching to IgG and IgA isotypes, respectively^{41,42}. We also found cross-
336 reactive memory B and T cells in healthy controls, as has been previously noted⁴³. It is difficult to
337 measure their contribution to the expanded populations of SARS-CoV-2-specific cells we found
338 in our CoV2⁺ cohorts, and therefore impossible to evaluate their protective capacity. However, we
339 can conclude that mild COVID-19 induces an expanded population of functionally diverse
340 memory lymphocytes compared to the cross-reactive pool present in our controls.

341

342 Studies of reinfection have yet to be done in humans, but macaques infected with SARS-CoV-2
343 were protected from rechallenge⁴⁴. This further suggests that the immune memory induced by mild

344 COVID-19 that we observed will be protective. While additional studies are needed to understand
345 variability of responses in a larger cohort and to determine how long memory to SARS-CoV-2
346 infection is truly maintained, our work suggests that mild COVID-19 induces persistent immune
347 memory poised for a coordinated, protective response to re-exposure that could contribute to herd
348 immunity and curtailing this pandemic.

349 **Main References:**

- 350 1 Wu, Z. & McGoogan, J. M. Characteristics of and Important Lessons From the
351 Coronavirus Disease 2019 (COVID-19) Outbreak in China: Summary of a Report of
352 72 314 Cases From the Chinese Center for Disease Control and Prevention. *JAMA* **323**,
353 1239-1242, doi:10.1001/jama.2020.2648 (2020).
- 354 2 Ruterbusch, M., Pruner, K. B., Shehata, L. & Pepper, M. In Vivo CD4(+) T Cell
355 Differentiation and Function: Revisiting the Th1/Th2 Paradigm. *Annu Rev Immunol* **38**,
356 705-725, doi:10.1146/annurev-immunol-103019-085803 (2020).
- 357 3 Knox, J. J., Myles, A. & Cancro, M. P. T-bet(+) memory B cells: Generation, function, and
358 fate. *Immunol Rev* **288**, 149-160, doi:10.1111/imr.12736 (2019).
- 359 4 Kim, C. C., Baccarella, A. M., Bayat, A., Pepper, M. & Fontana, M. F. FCRL5(+) Memory
360 B Cells Exhibit Robust Recall Responses. *Cell Rep* **27**, 1446-1460 e1444,
361 doi:10.1016/j.celrep.2019.04.019 (2019).
- 362 5 Nellore, A. *et al.* Fcrl5 and T-bet define influenza-specific memory B cells that predict
363 long-lived antibody responses. *bioRxiv*, 643973, doi:10.1101/643973 (2019).
- 364 6 Schmidt, M. E. & Varga, S. M. The CD8 T Cell Response to Respiratory Virus Infections.
365 *Frontiers in Immunology* **9**, doi:10.3389/fimmu.2018.00678 (2018).
- 366 7 Hoffmann, M. *et al.* SARS-CoV-2 Cell Entry Depends on ACE2 and TMPRSS2 and Is
367 Blocked by a Clinically Proven Protease Inhibitor. *Cell* **181**, 271-280 e278,
368 doi:10.1016/j.cell.2020.02.052 (2020).
- 369 8 Shi, R. *et al.* A human neutralizing antibody targets the receptor binding site of SARS-
370 CoV-2. *Nature*, doi:10.1038/s41586-020-2381-y. (2020).

- 371 9 Robbiani, D. F. *et al.* Convergent antibody responses to SARS-CoV-2 in convalescent
372 individuals. *Nature* **18**, 18, doi: <https://dx.doi.org/10.1038/s41586-020-2456-9> (2020).
- 373 10 Long, Q.-X. *et al.* Antibody responses to SARS-CoV-2 in patients with COVID-19. *Nature*
374 *Medicine* **26**, 845-848, doi:10.1038/s41591-020-0897-1 (2020).
- 375 11 Wölfel, R. *et al.* Virological assessment of hospitalized patients with COVID-2019. *Nature*
376 **581**, 465-469, doi:10.1038/s41586-020-2196-x (2020).
- 377 12 Mathew, D. *et al.* Deep immune profiling of COVID-19 patients reveals distinct
378 immunotypes with therapeutic implications. *Science (New York, NY)*,
379 doi:10.1126/science.abc8511. (2020).
- 380 13 Slifka, M. K. & Ahmed, R. Long-term antibody production is sustained by antibody-
381 secreting cells in the bone marrow following acute viral infection. *Ann N Y Acad Sci* **797**,
382 166-176, doi:10.1111/j.1749-6632.1996.tb52958.x (1996).
- 383 14 Knox, J. J. *et al.* T-bet⁺ B cells are induced by human viral infections and dominate the
384 HIV gp140 response. *JCI Insight* **2**, doi:10.1172/jci.insight.92943 (2017).
- 385 15 Ma, H. *et al.* Serum IgA, IgM, and IgG responses in COVID-19. *Cellular & Molecular*
386 *Immunology* **17**, 773-775, doi:10.1038/s41423-020-0474-z (2020).
- 387 16 Tan, C. W. *et al.* A SARS-CoV-2 surrogate virus neutralization test based on antibody-
388 mediated blockage of ACE2–spike protein–protein interaction. *Nature Biotechnology*,
389 doi:10.1038/s41587-020-0631-z (2020).
- 390 17 Krishnamurty, A. T. *et al.* Somatically Hypermutated Plasmodium-Specific IgM(+)
391 Memory B Cells Are Rapid, Plastic, Early Responders upon Malaria Rechallenge.
392 *Immunity* **45**, 402-414, doi:10.1016/j.immuni.2016.06.014 (2016).

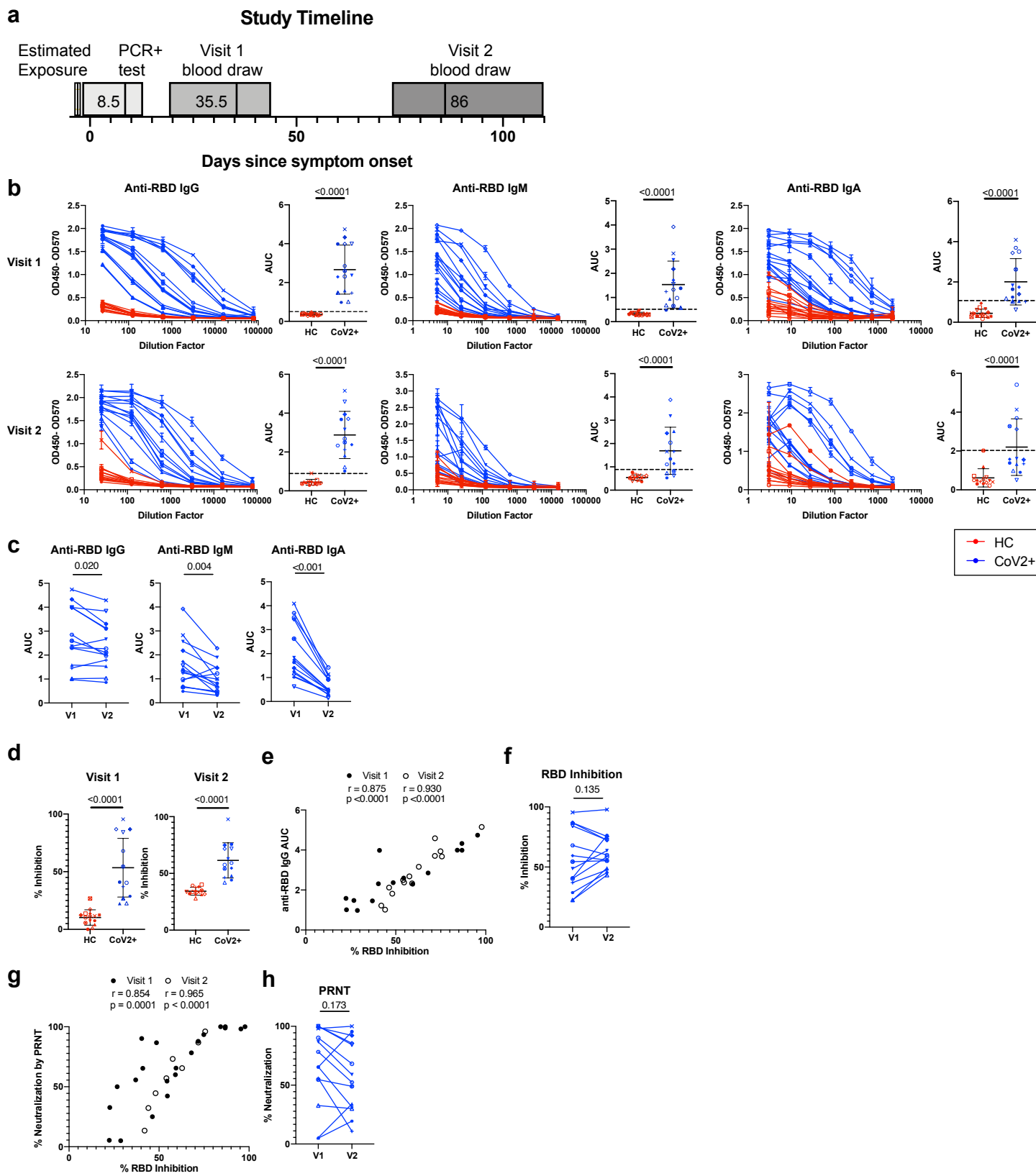
- 393 18 Ladner, J. T. *et al.* Epitope-resolved profiling of the SARS-CoV-2 antibody response
394 identifies cross-reactivity with an endemic human CoV. *bioRxiv*, 2020.2007.2027.222943,
395 doi:10.1101/2020.07.27.222943 (2020).
- 396 19 Braun, J. *et al.* SARS-CoV-2-reactive T cells in healthy donors and patients with COVID-
397 19. *Nature*, doi:10.1038/s41586-020-2598-9 (2020).
- 398 20 Weiskopf, D. *et al.* Phenotype and kinetics of SARS-CoV-2-specific T cells in COVID-19
399 patients with acute respiratory distress syndrome. *Sci Immunol* **5**,
400 doi:10.1126/sciimmunol.abd2071 (2020).
- 401 21 Knox, J. J., Kaplan, D. E. & Betts, M. R. T-bet-expressing B cells during HIV and HCV
402 infections. *Cell Immunol* **321**, 26-34, doi:10.1016/j.cellimm.2017.04.012 (2017).
- 403 22 Weisel, F. & Shlomchik, M. Memory B Cells of Mice and Humans. *Annual Review of*
404 *Immunology* **35**, 255-284, doi:10.1146/annurev-immunol-041015-055531 (2017).
- 405 23 Bentebibel, S. E. *et al.* Induction of ICOS⁺CXCR3⁺CXCR5⁺ TH cells correlates with
406 antibody responses to influenza vaccination. *Sci Transl Med* **5**, 176ra132,
407 doi:10.1126/scitranslmed.3005191 (2013).
- 408 24 Reiss, S. *et al.* Comparative analysis of activation induced marker (AIM) assays for
409 sensitive identification of antigen-specific CD4 T cells. *PLoS One* **12**, e0186998,
410 doi:10.1371/journal.pone.0186998 (2017).
- 411 25 Vinuesa, C. G., Linterman, M. A., Yu, D. & MacLennan, I. C. Follicular Helper T Cells.
412 *Annu Rev Immunol* **34**, 335-368, doi:10.1146/annurev-immunol-041015-055605 (2016).
- 413 26 Pepper, M. & Jenkins, M. K. Origins of CD4(+) effector and central memory T cells. *Nat*
414 *Immunol* **12**, 467-471, doi:10.1038/ni.2038 (2011).

- 415 27 Juno, J. A. *et al.* Humoral and circulating follicular helper T cell responses in recovered
416 patients with COVID-19. *Nature medicine*, doi:10.1038/s41591-020-0995-0. (2020).
- 417 28 Le Bert, N. *et al.* SARS-CoV-2-specific T cell immunity in cases of COVID-19 and SARS,
418 and uninfected controls. *Nature*, doi:10.1038/s41586-020-2550-z (2020).
- 419 29 Alsoussi, W. B. *et al.* A Potently Neutralizing Antibody Protects Mice against SARS-CoV-
420 2 Infection. *J Immunol*, doi:10.4049/jimmunol.2000583 (2020).
- 421 30 Hanke, L. *et al.* An alpaca nanobody neutralizes SARS-CoV-2 by blocking receptor
422 interaction. *bioRxiv*, 2020.2006.2002.130161, doi:10.1101/2020.06.02.130161 (2020).
- 423 31 Tang, F. *et al.* Lack of Peripheral Memory B Cell Responses in Recovered Patients with
424 Severe Acute Respiratory Syndrome: A Six-Year Follow-Up Study. *The Journal of*
425 *Immunology* **186**, 7264-7268, doi:10.4049/jimmunol.0903490 (2011).
- 426 32 Wu, L. P. *et al.* Duration of antibody responses after severe acute respiratory syndrome.
427 *Emerg Infect Dis* **13**, 1562-1564, doi:10.3201/eid1310.070576 (2007).
- 428 33 Seow, J. *et al.* Longitudinal evaluation and decline of antibody responses in SARS-CoV-2
429 infection. *medRxiv*, 2020.2007.2009.20148429, doi:10.1101/2020.07.09.20148429 (2020).
- 430 34 Perreault, J. *et al.* Longitudinal analysis of the humoral response to SARS-CoV-2 spike
431 RBD in convalescent plasma donors. *bioRxiv*, 2020.2007.2016.206847,
432 doi:10.1101/2020.07.16.206847 (2020).
- 433 35 Wajnberg, A. *et al.* SARS-CoV-2 infection induces robust, neutralizing antibody responses
434 that are stable for at least three months. *medRxiv*, 2020.2007.2014.20151126,
435 doi:10.1101/2020.07.14.20151126 (2020).

- 436 36 Isho, B. *et al.* Evidence for sustained mucosal and systemic antibody responses to SARS-
437 CoV-2 antigens in COVID-19 patients. *medRxiv*, 2020.2008.2001.20166553,
438 doi:10.1101/2020.08.01.20166553 (2020).
- 439 37 Plotkin, S. A. Correlates of protection induced by vaccination. *Clin Vaccine Immunol* **17**,
440 1055-1065, doi:10.1128/CVI.00131-10 (2010).
- 441 38 Grifoni, A. *et al.* Targets of T Cell Responses to SARS-CoV-2 Coronavirus in Humans
442 with COVID-19 Disease and Unexposed Individuals. *Cell* **181**, 1489-1501 e1415,
443 doi:10.1016/j.cell.2020.05.015 (2020).
- 444 39 Rubtsova, K., Rubtsov, A. V., van Dyk, L. F., Kappler, J. W. & Marrack, P. T-box
445 transcription factor T-bet, a key player in a unique type of B-cell activation essential for
446 effective viral clearance. *Proc Natl Acad Sci U S A* **110**, E3216-3224,
447 doi:10.1073/pnas.1312348110 (2013).
- 448 40 Lee, Y. K. *et al.* Late developmental plasticity in the T helper 17 lineage. *Immunity* **30**, 92-
449 107, doi:10.1016/j.immuni.2008.11.005 (2009).
- 450 41 Peng, S. L., Szabo, S. J. & Glimcher, L. H. T-bet regulates IgG class switching and
451 pathogenic autoantibody production. *Proc Natl Acad Sci U S A* **99**, 5545-5550,
452 doi:10.1073/pnas.082114899 (2002).
- 453 42 Hirota, K. *et al.* Plasticity of Th17 cells in Peyer's patches is responsible for the induction
454 of T cell-dependent IgA responses. *Nat Immunol* **14**, 372-379, doi:10.1038/ni.2552 (2013).
- 455 43 Mateus, J. *et al.* Selective and cross-reactive SARS-CoV-2 T cell epitopes in unexposed
456 humans. *Science*, doi:10.1126/science.abd3871 (2020).
- 457 44 Chandrashekar, A. *et al.* SARS-CoV-2 infection protects against rechallenge in rhesus
458 macaques. *Science*, doi:10.1126/science.abc4776 (2020).

459 45 Erasmus, J. H. *et al.* Single-dose replicating RNA vaccine induces neutralizing antibodies
460 against SARS-CoV-2 in nonhuman primates. *bioRxiv*, doi:10.1101/2020.05.28.121640
461 (2020).
462

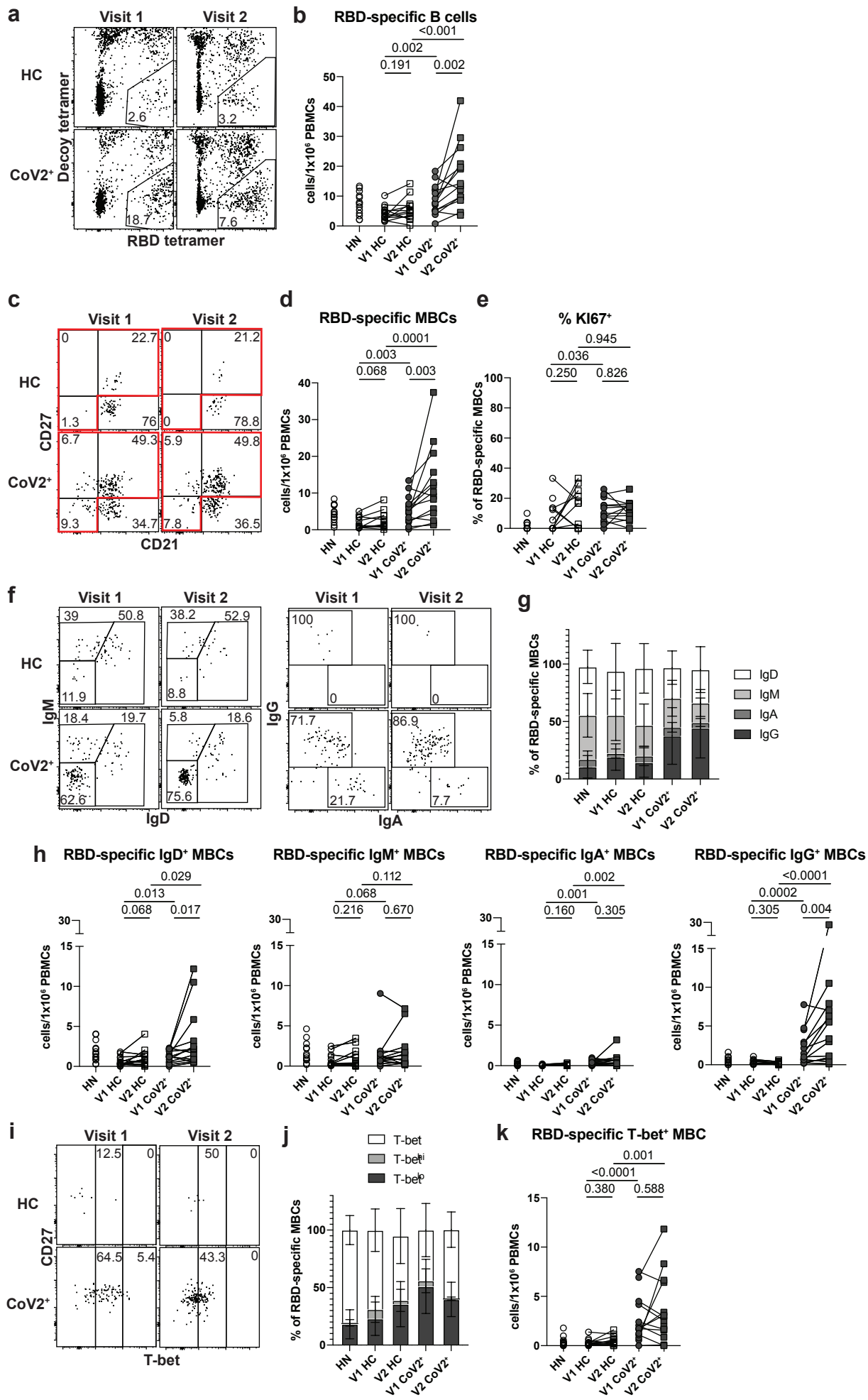
Figure 1



463 **Figure 1: SARS-CoV-2-specific plasma antibodies at two memory time points.**

464 **a)** Study timeline. Range indicated by box and median indicated by line for each event. **b)**
465 ELISA dilution curves and AUC for anti-RBD IgG (left), IgM (center), and IgA (right) from
466 healthy control (HC) and previously SARS-CoV-2-infected (CoV2⁺) plasma samples at Visit 1
467 (V1) and Visit 2 (V2). Dashed line indicates mean + 3 SD of the HC AUC values. Each symbol
468 is a different individual and is consistent throughout the figure. **c)** V2 CoV2⁺ AUC values were
469 normalized to V1 samples run with V2 samples and AUC for each CoV2⁺ individual from V1
470 and V2 are paired. **d)** Percent inhibition of RBD binding to ACE2 by plasma at 1:10 dilution. **e)**
471 Spearman correlation between percent RBD inhibition at a 1:10 plasma dilution and anti-RBD
472 IgG AUC. **f)** CoV2⁺ percent RBD inhibition at 1:10 plasma dilution normalized and paired as in
473 c). **g)** Spearman correlation between percent RBD inhibition at a 1:10 plasma dilution and
474 percent virus neutralization by PRNT at a 1:160 plasma dilution. **h)** CoV2⁺ percent virus
475 neutralization by PRNT at a 1:160 plasma dilution normalized and paired as in c). Statistical
476 significance for unpaired data determined by two-tailed Mann-Whitney tests and, for paired data,
477 by two-tailed Wilcoxon signed-rank tests. Error bars represent mean and SD (V1 HC n=15, V2
478 HC n=14, V1 CoV2⁺ n=15, V2 CoV2⁺ n=14).

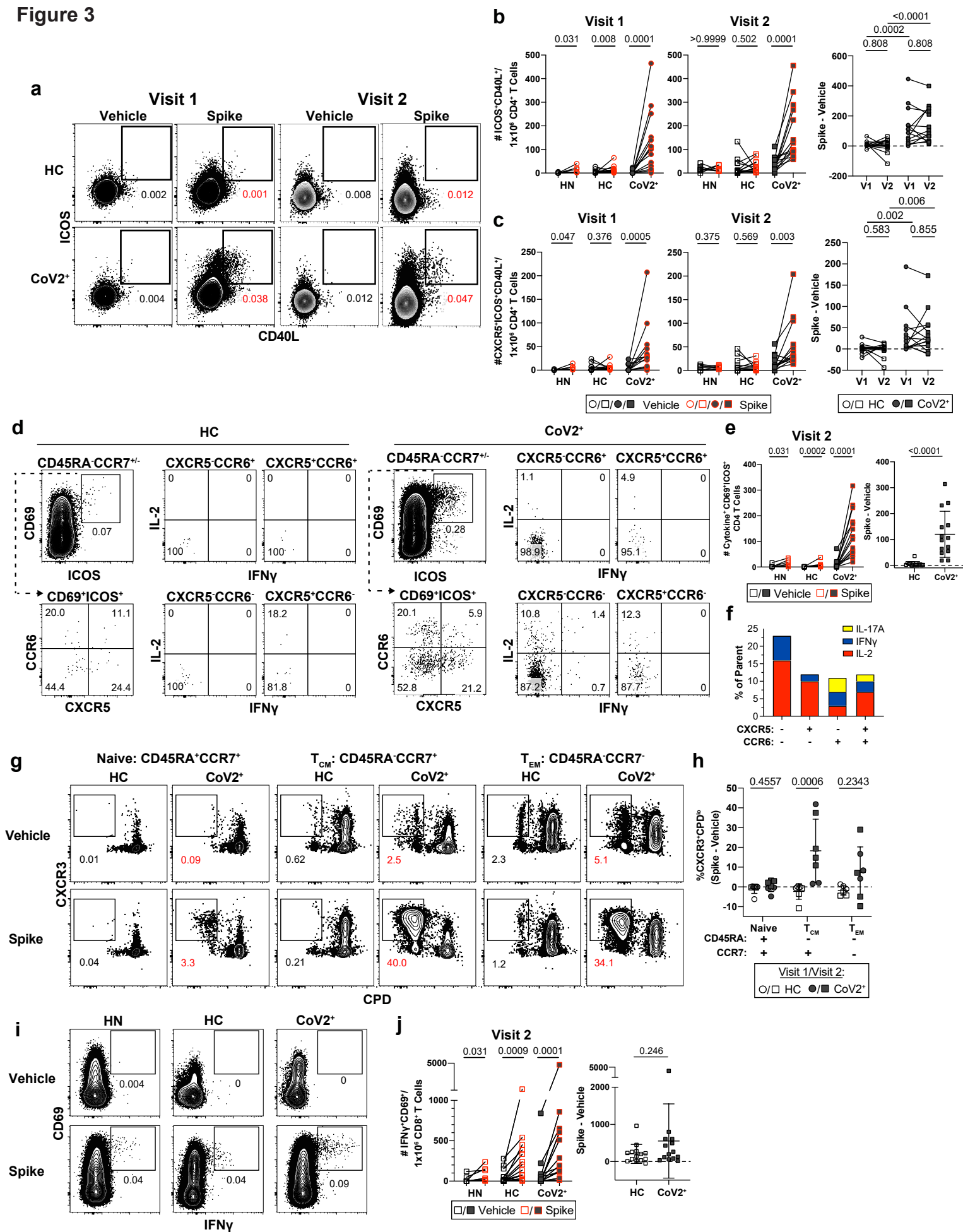
Figure 2



479 **Figure 2: RBD-specific MBCs form and persist in PBMCs post-mild COVID-19.**

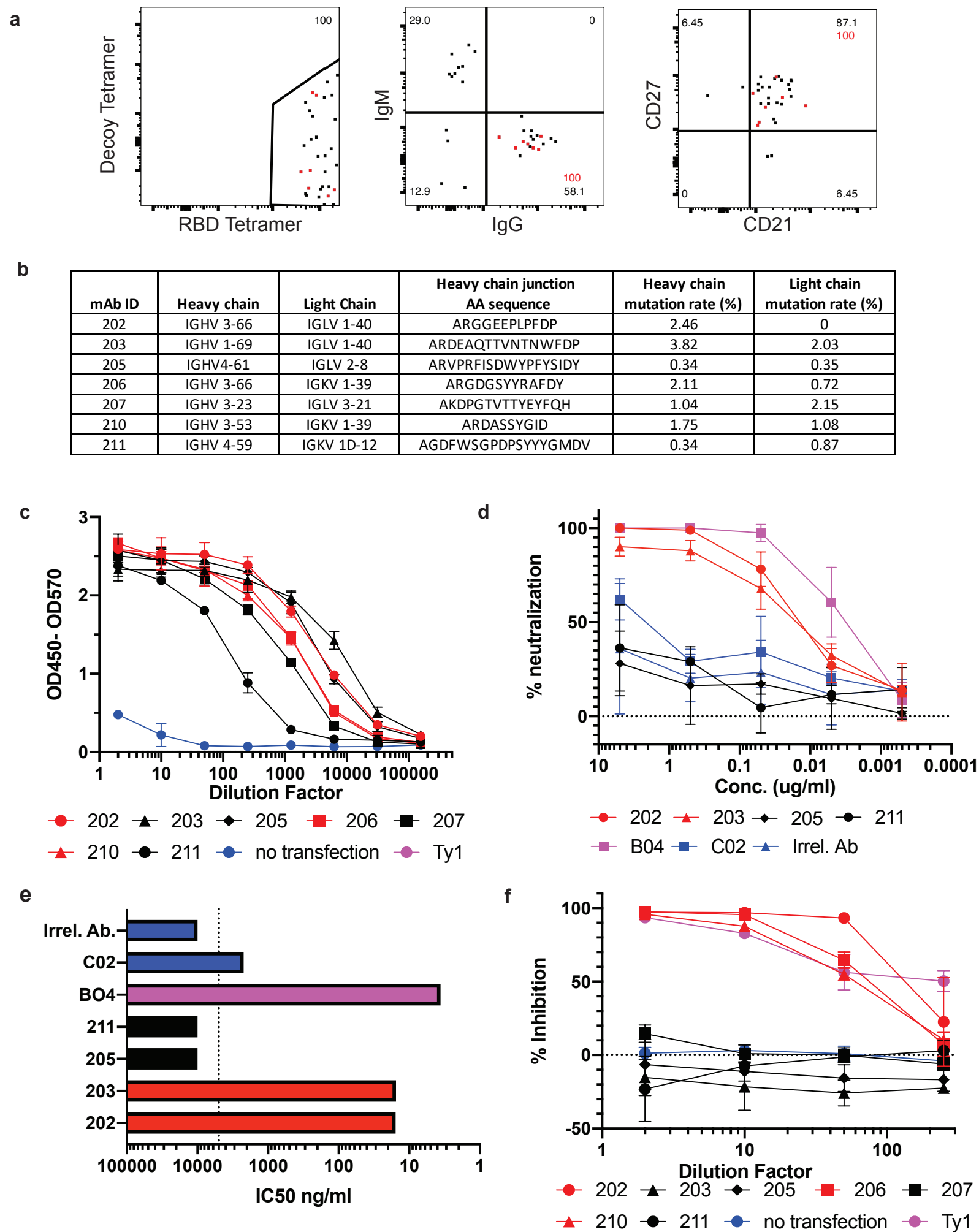
480 **a)** Representative gating of Live CD3⁻CD14⁻CD16⁻ cells for SARS-CoV-2 RBD-specific cells
481 (RBD tetramer⁺Decoy⁻) and **b)** number of RBD-specific B cells (RBD tetramer⁺Decoy⁻CD20⁺)
482 from SARS-CoV-2-recovered (CoV2⁺) and healthy control (HC) PBMCs at Visit 1 (V1) and
483 Visit 2 (V2). Gating strategy shown in Extended Data Figure 5c. **c)** Representative gating and **d)**
484 Number of RBD-specific memory B cells (MBCs: CD21⁺CD27⁺/CD21⁻CD27⁺/CD21⁻CD27⁻
485 populations outlined in red in c)(HN n=14, V1 HC n=12, V2 HC n=13 , V1 CoV2⁺ n=15, V2
486 CoV2⁺ n=14). **e)** Frequency of cycling (Ki67⁺) RBD-specific MBCs. **f)** Representative gating, **g)**
487 frequency (HN n=14, V1 HC n=12, V2 HC n=13, V1 CoV2⁺ n=15, V2 CoV2⁺ n=14) and **h)**
488 number of RBD-specific MBCs expressing the BCR isotypes IgD, IgM, IgA and IgG. **i)**
489 Representative gating, **j)** frequency and **k)** number of RBD-specific MBCs expressing T-bet.
490 Statistical significance determined by two-tailed, Mann-Whitney test (HC vs. CoV2⁺) and two-
491 tailed Wilcoxon signed rank test (V1 vs V2). Error bars represent mean and SD (HN n=14, V1
492 HC n=15, V2 HC n=15, V1 CoV2⁺ n=15, V2 CoV2⁺ n=14 unless otherwise noted, 2
493 experiments).

Figure 3



494 **Figure 3: *Ex vivo* reactivation of spike-specific CD4⁺ T Cells reveals durable and functional**
495 **immune memory in SARS-CoV-2-recovered individuals.**

496 **a)** Representative flow cytometry plots 20 hours after Vehicle control or Spike-stimulation of
497 PBMCs from HC and CoV2⁺ individuals demonstrating T cell upregulation of CD40L and ICOS
498 on CD45RA⁻CD4⁺ T cells. **b)** Enumeration of total CD40L⁺ICOS⁺ and **c)**
499 CXCR5⁺CD40L⁺ICOS⁺ (cTfh) per 1e6 CD4⁺ T Cells and paired CoV2⁺ data from Visit 1 and
500 Visit 2 represented as frequency of spike minus vehicle. **d)** Representative flow cytometry plots
501 and **e)** number of CD69⁺ICOS⁺ CD4⁺ T Cells producing intracellular cytokines and number
502 producing cytokine after incubation with spike minus number after incubation with vehicle. **f)**
503 Relative distribution of effector cytokine production in memory T Cell compartments (CCR6^{+/+}-
504 cTfh and non-cTfh) following *ex vivo* stimulation for 20 hrs; (IFN- γ ; blue) (IL-2; red) (IL-17A;
505 yellow) from **(d)**. **g)** Antigen-specific T cell proliferation of sorted CD4⁺ naive or memory T
506 cells in control and CoV2⁺ PBMCs. Proliferation following 5-6 day co-culture with SARS-CoV-
507 2 spike protein-pulsed autologous monocytes. **h)** Antigen-specific expansion represented as
508 frequency of spike minus vehicle, CXCR3⁺CPD^{low} responding cells. **i)** Representative flow
509 cytometry plots and **j)** quantification of spike-specific CD8⁺ T Cells in control and Cov2⁺
510 PBMCs stimulated with SARS-CoV-2 spike protein. **a-h)** Significance was determined by
511 Kruskal-Wallis test correcting for multiple comparisons using FDR two-stage method. Adjusted
512 p values are reported. **i-j)** Significance was determined by two-tailed, non-parametric Mann-
513 Whitney tests. **a-j)** Data represented as mean and SD; Each symbol represents one donor. **a-f, i-j)**
514 n=7 HN, n=14 HC, n=14 CoV2⁺(2 experiments). **g-h)** n=3 V1 HC, n=4 V2 HC, n=3 V1 CoV2⁺,
515 n=4 V2 CoV2⁺ (2 experiments).



516 **Figure 4. Generation of neutralizing antibodies by RBD-specific MBCs.**

517 **a)** Flow plots of index sorted RBD-tetramer specific B cells (gating scheme in Extended Data
518 Figure 7a). B cell receptors (BCRs) cloned from cells shown in red. **b)** Heavy and light chain
519 gene usage, somatic hypermutation rate and VDJ junction sequence of cloned BCRs. **c)** Anti-
520 RBD ELISA of culture supernatants from cells transfected to express one of the monoclonal
521 antibodies compared to a known RBD-binding and neutralizing antibody (Ty1) and supernatant
522 from untransfected cells (no transfection). **d)** Neutralization capacity of purified monoclonal
523 antibodies as measured by PRNT. BO4 and CO2 are previously identified strong and weak
524 neutralizing murine antibodies. **e)** IC50 values of antibodies calculated from PRNT. Dotted line
525 represents the limit of detection. **f)** Inhibition of RBD-ACE2 binding by culture supernatants
526 from antibody transfections (antibodies with high inhibitory capacity shown in red).

527 **Methods:**

528 **Ethics Statement**

529 This study was approved by the University of Washington Institutional Review Board (Gale Lab,
530 IRB 00009810). Informed consent was obtained from all enrolled participants. Samples were de-
531 identified prior to transfer to the Pepper Lab.

532 **Study Participants:**

533 The study was conceptualized utilizing a prospective case-control design. Cases and controls were
534 identified from a cross-sectional cohort study that recruited via print and online advertising from
535 the Seattle metropolitan area (**E.D. Table 1**). Cases (n=15) were selected based on a reported
536 history of a positive SARS-CoV-2 PCR nasal swab. Controls (n=17) were selected based on having
537 no prior positive SARS-CoV-2 PCR nasal swab and having no detectable SARS-CoV-2 RBD- or
538 S-specific IgG or IgM plasma antibodies (within mean + 3 SD of 5 de-identified plasma samples
539 drawn prior to 2020 generously donated by Wesley C. Van Voorhis). At the time of enrollment,
540 information was collected from all participants regarding recent illness symptoms and severity.
541 All CoV2⁺ cases reported at least one symptom but all were classified as mild disease, as none
542 required hospitalization. Historical negative control PBMCs (n=14) were sourced from the BRI
543 PBMC repository. Samples were drawn prior to 2020 and age and sex matched to the CoV2⁺ cases.

544

545 **Peripheral blood mononuclear cell (PBMC) and plasma collection**

546 6-10 milliliters of venous blood from study volunteers were collected in EDTA tubes and spun at
547 1500xg for 10 minutes. Plasma was collected, heat-inactivated at 56°C for 30 minutes, aliquoted

548 and stored at -80°C. The cellular fraction was resuspended in PBS and PBMC were separated from
549 RBC using Sepmate PBMC Isolation Tubes (STEMCELL Technologies) according to
550 manufacturer's instruction and frozen at -80°C before being stored in liquid nitrogen. PBMCs were
551 thawed at 37°C and washed twice before use.

552

553 **SARS-CoV-2 Protein Production and Purification**

554 *Plasmid construction*

555 The SARS-CoV-2 S^B (BEI NR-52422) construct was synthesized by GenScript into pcDNA3.1-
556 with an N-terminal mu-phosphatase signal peptide and a C-terminal octa-histidine tag
557 (GHHHHHHHH). The boundaries of the construct are N-₃₂₈RFPN₃₃₁ and C-₅₂₈KKST₅₃₁. The
558 SARS-CoV-2 S-2P ectodomain trimer (GenBank: YP_009724390.1, BEI NR-52420; cite PMID
559 32155444) was synthesized by GenScript into pCMV with an N-terminal mu-phosphatase signal
560 peptide and a C-terminal TEV cleavage site (GSGRENLYPQG), T4 fibritin foldon
561 (GGGSGYIPEAPRDGQAYVRKDGEWLLSTPL), and octa-histidine tag (GHHHHHHHHH).
562 The construct contains the 2P mutations (proline substitutions at residues 986 and 987; PMID
563 28807998) and an ₆₈₂SGAG₆₈₅ substitution at the furin cleavage site. A pCAGGS vector containing
564 the spike protein RBD from SARS-CoV-2 (Wuhan-Hu-1 isolate) was generously provided by
565 Florian Krammer.

566

567 *Transient expression*

568 Constructs were produced in Expi293F cells grown in suspension using Expi293F expression
569 medium (Life technologies) at 33°C, 70% humidity, and 8% CO₂ rotating at 150 rpm. The cultures
570 were transfected using PEI-MAX (Polyscience) with cells grown to a density of 3.0 million cells

571 per mL and cultivated for 3 days. Supernatants was clarified by centrifugation (5 minutes at 4000
572 rcf), addition of PDADMAC solution to a final concentration of 0.0375% (Sigma Aldrich,
573 #409014), and a second spin (5 minutes at 4000 rcf).

574

575 *Purification of His-tagged proteins*

576 Proteins were purified from clarified supernatants via a batch bind method where each supernatant
577 was supplemented with 1 M Tris-HCl pH 8.0 to a final concentration of 45 mM and 5 M NaCl to
578 a final concentration of ~310 mM). Talon cobalt affinity resin (Takara) was added to the treated
579 supernatants and allowed to incubate for 15 minutes with gentle shaking. Resin was collected using
580 vacuum filtration using a 0.2 µm filter and transferred to a gravity column. The resin was washed
581 with 20 mM Tris pH 8.0, 300 mM NaCl, and the protein was eluted with three column volumes of
582 20 mM Tris pH 8.0, 300 mM imidazole, 300 mM NaCl. The batch bind process was then repeated
583 and the first and second elutions combined. SDS-PAGE was used to assess purity. Purified S-2P
584 trimer was concentrated to ~1 mg/mL and dialyzed into 50 mM Tris pH 8, 150 mM NaCl, 0.25%
585 L-Histidine, 5% glycerol in a hydrated 10k molecular weight cutoff dialysis cassette (Thermo
586 Scientific). The purified RBD protein was dialyzed into 50 mM Tris pH 7, 185 mM NaCl, 100
587 mM Arginine, 4.5% glycerol, 0.75% w/v CHAPS. Due to inherent instability, S-2P was
588 immediately flash frozen and stored at -80°C.

589

590 **Tetramer generation**

591 Recombinant trimeric spike and the RBD domain were both biotinylated using a EZ-Link Sulfo-
592 NHS-LC Biotinylation Kit (ThermoFisher), tetramerized with streptavidin-PE (Agilent) and stored
593 in 50% glycerol at -20°C as previously described¹⁷. Decoy reagent was generated by tetramerizing

594 an irrelevant biotinylated protein with SA-PE previously conjugated to AF647 using an Alexa
595 Fluor 647 Antibody Labeling Kit (ThermoFisher).

596

597 **Tetramer validation in mice**

598 Adult C57BL/6j mice (The Jackson Laboratory) were immunized with 50ug SARS-CoV-2 RBD
599 in CFA in the footpad and, 7-10 days later, popliteal lymph nodes were dissected, mashed and
600 stained in 10nM decoy-PE-APC tetramer and then 10nM RBD-PE as described¹⁷ and as
601 described below for immunophenotyping B cells. Cells stained for surface markers as indicated
602 **(Supplemental Table 1)** and run on the LSRII (BD). Data analyzed with FlowJo10 (Becton
603 Dickinson). Mice were purchased from The Jackson Laboratory and maintained under specific
604 pathogen free conditions at the University of Washington. All mouse experiments were
605 performed in accordance with the University of Washington Institutional Care and Use
606 Committee guidelines.

607

608 **ELISA**

609 96-well plates (Corning) were coated with 2 ug/mL of recombinant SARS-CoV-2 RBD or trimeric
610 spike protein diluted in PBS and incubated at 4°C overnight. Plates were washed with PBS-T (PBS
611 containing 0.05% Tween-20) and incubated with blocking buffer (PBS-T and 3% milk) for 1 hour
612 at room temperature (RT). Serum, culture supernatants or monoclonal antibodies were serially
613 diluted in dilution buffer (PBS-T and 1% milk) in triplicate, added to plates, and incubated at RT
614 for 2 hours. Secondary antibodies were diluted in dilution buffer as follows: anti-human IgG-HRP
615 (Jackson ImmunoResearch) at 1:3000, anti-human IgM-HRP (Southern Biotech) at 1:3000, or
616 anti-human IgA-HRP (Southern Biotech) at 1:1500. Plates were incubated with secondary

617 antibodies for 1 hour at RT, then detected with 1X TMB (Invitrogen) and quenched with 1M HCl.
618 Sample optical density (OD) was measured by a spectrophotometer at 450nm and 570nm. CR3022,
619 a human SARS-CoV antibody previously determined to cross-react with SARS-CoV-2 was used
620 as a positive control. IgG in culture supernatants was measured using a Human IgG ELISA Kit
621 (Stemcell) according to the manufacturer's instructions. Data was analysed in Prism (GraphPad).

622

623 **Receptor-binding inhibition assay**

624 96-well plates (Corning) were coated with 5 ug/mL of recombinant human ACE2-Fc diluted in
625 100mM carbonate-bicarbonate buffer (pH 9.6) and incubated at 4°C overnight. Plates were washed
626 with PBS-T and incubated with blocking buffer for 1 hour at RT. Plasma or monoclonal antibody
627 supernatants were serially diluted in triplicate in dilution buffer and incubated with 18ng of
628 recombinant SARS-CoV-2 RBD-HRP (conjugated using Abcam HRP conjugation kit) for 1 hour
629 at 37C. Blocked plates were washed and incubated with the pre-incubated serum and RBD-HRP
630 for 1 hour at RT, then detected with TMB and 1M HCl. OD was measured by a spectrophotometer
631 at 450nm and 570nm. RBD-HRP alone and serum with no RBD-HRP incubation were used as
632 controls. The % inhibition was calculated as $(1 - \text{Sample OD value} / \text{Average Negative Control OD}$
633 $\text{value}) \times 100$. Data was analysed in Prism (GraphPad).

634

635 **Plaque reduction neutralization test (PRNT)**

636 PRNT assays were performed as previously described⁴⁵. Briefly, heat inactivated plasma was
637 diluted 1:5 followed by four 4-fold serial dilutions and monoclonal antibodies were diluted 1:10
638 followed by 4 10-fold serial dilution and mixed 1:1 with 600 PFU/ml SARS-CoV-2 WA-1 (BEI
639 resources) in PBS+0.3% cold water fish skin gelatin (Sigma). After 30 minutes of incubation at

640 37°C, the plasma/virus mixtures were added to 12 well plates of Vero cells and incubated for 1
641 hour at 37C, rocking every 15 minutes. All dilutions were done in duplicate, along with virus only
642 and no virus controls. Plates were then washed with PBS and overlaid with a 1:1 mixture of 2.4%
643 Avicel RC-591 (FMC) and 2X MEM (ThermoFisher) supplemented with 4% heat-inactivated FBS
644 and Penicillin/Streptomycin (Fisher Scientific.) After a 48 hour incubation, the overlay was
645 removed, plates were washed with PBS, fixed with 10% formaldehyde (Sigma-Aldrich) in PBS
646 for 30 minutes at room temp and stained with 1% crystal violet (Sigma-Aldrich) in 20% EtOH. %
647 Neutralization was calculated as $(1 - \# \text{ sample plaques} / \# \text{ positive control plaques}) \times 100$. Data was
648 analysed in Prism (GraphPad) and IC50 was calculated by sigmoidal interpolation method.

649

650 **Cell Enrichment, Stimulations and Flow Cytometry**

651 *Immunophenotyping and sorting RBD-specific B cells*

652 Thawed PBMCs were first stained with Decoy tetramer and then with RBD tetramer prior to
653 incubation with anti-PE magnetic beads and magnetic bead enrichment (Miltenyi Biotec) as
654 previously described.¹⁷ Bound cells were stained with surface antibodies (**SI Table 1**) and, if
655 required, were fixed/permeabilized using eBioscience FoxP3 Fix/Perm kit (ThermoFisher; 00-
656 5521-00) for 30 minutes, followed by incubation with intracellular antibodies (**SI Table 1**). Stained
657 samples were run on a LSRII flow cytometer and analyzed using FlowJo (Becton Dickinson). For
658 B cells sorting experiments, single tetramer-specific B cells were indexed sorted on a FACSAriaII
659 cell sorter and collected in a 96-well PCR plate containing SMART-Seq v4 capture buffer (Takara
660 Bio).

661

662 *Immunophenotyping of PBMCs*

663 For surface phenotyping, total PBMCs (innate cells) or PBMCs from the negative fraction of the
664 antigen-specific B Cell magnetic columns (for lymphocytes) were washed and incubated with
665 fluorescently conjugated antibodies. Staining for cTfh analyses were performed as follows:
666 chemokine-receptors and transcription factors (40 minutes, RT), surface antigens (20 minutes,
667 4°C)(SI Table 1). Intracellular staining was performed using eBioscience FoxP3 Fix/Perm kit
668 (ThermoFisher; 00-5521-00)(SI Table 1). For detection of intracellular cytokine production,
669 PBMC were stimulated with 50 ng/ml phorbol 12-myristate 13-acetate (Sigma-Aldrich) and 1
670 µg/ml Ionomycin (Sigma-Aldrich; I06434) with 10 µg/ml Brefeldin A (Sigma-Aldrich; B6542)
671 and 1x dose GolgiStop/monensin (Becton Dickinson; 554724) for 4 hours. Permeabilization and
672 fixation was performed using Cytofix/Cytoperm (Becton Dickinson; RUO 554714). Intracellular
673 stains were performed for 30 minutes at 4°C (SI Table 1). Flow cytometry analysis of innate
674 immune populations was done on 0.5-1 million PBMCs before fraction isolation. Data was
675 acquired on a Cytex Aurora or BD LSR Fortessa and analyzed using FlowJo10 software (Becton
676 Dickinson).

677

678 *Ex-Vivo spike Protein Stimulation of Peripheral Blood T Cells*

679 PBMCs from the negative fraction of antigen-specific B Cell magnetic columns were washed and
680 resuspended to 4×10^6 cells/mL with complete RPMI with 10mM HEPES (ThermoFisher;
681 22400097) supplemented with 10% FBS, 2Me, Pen-Strep, and L-Glutamine. Spike-stimulated
682 PBMCs were incubated with 2µg/mL full-length recombinant spike protein resuspended in PBS +
683 5% glycerol. Unstimulated controls received equivalent volume of PBS + 5% glycerol vehicle.
684 Both conditions were left for 20 hours at 37°C, 5-8% CO₂, with addition of 10 µg/ml Brefeldin A
685 (Sigma-Aldrich; B6542) and 1x dose GolgiStop/monensin (Becton Dickinson; 554724) for the

686 final 5 hours to allow for intracellular detection of cytokines. Positive controls were stimulated
687 with PMA/Ionomycin (see above) for 5 hours in the presence of Brefeldin-A and Monensin.
688 Staining was performed as follows: chemokine-receptors (40 minutes, RT), surface antigens and
689 cytokines (20 minutes, 4°C) (**SI Table 1**). Cells were run on the Cytex Aurora and analyzed using
690 FlowJo (Becton Dickenson).

691

692 *Antigen-specific T cell proliferation*

693 Starting with PBMC from healthy control or CoV2⁺ individuals, cell proliferation dye (CPD)-
694 labeled, 1.25uM (ThermoFisher; 65-0840-85), sorted naïve or memory T cell subsets (5×10^4)
695 were co-cultured in round-bottomed 96-well plates with irradiated autologous monocytes (5000
696 rads, 5×10^4), and provided either full-length recombinant human spike protein (2.5ug/mL)
697 resuspended in 5% PBS-glycerol or vehicle control. Cultures were supplemented with 5U/mL
698 recombinant human IL-2 (Biolegend; 589104). Cellular proliferation was assessed after 5-6 days
699 by flow cytometry (**SI Table 1**) as above and analyzed using FlowJo10 (Becton Dickenson). The
700 percentage of CXCR3⁺CPD^{lo} cells (defined as cells that had undergone 3 or more divisions)
701 represented as Spike - Vehicle is calculated by subtracting the vehicle control proliferation from
702 spike-treated proliferation.

703

704 **Monoclonal antibody generation**

705 *BCR sequencing and cloning*

706 Amplification of cDNA was performed using SMART-Seq v4 (Takara Bio) at half reaction
707 volume for each sorted cell. BCR chains were amplified in a multiplex PCR using half reactions
708 of DreamTaq (Thermo Fisher) and 1.25 ul of resulting cDNA with 3' primers for constant regions

709 of IgM, IgA, (5'-GGAAGGAAGTCCTGTGCGAGGC-3', 5'-
710 GGAAGAAGCCCTGGACCAGGC-3', Wardemann and Busse, 2019) IgG, IgK, IgL (5'-
711 TCTTGTCACCTTGGTGTGCT'-3', 5'-GTTTCTCGTAGTCTGCTTTGCTCA-3', 5'-
712 CACCAGTGTGGCCTTGTGGCTTG-3', Smith et al, 2009) and a 5' primer for the template
713 switch sequence (5'-GTGGTATCAACGCAGAGTACATGGG-3'). Thermocycler conditions
714 were 95 °C for 2 min, 30 cycles of 95 °C for 30s, 57 °C for 30s and 72 °C for 1 min.. Resulting
715 PCR products were cleaned using 5 ul of PCR reaction, 1 ul FastAP (Thermo Fisher), and 0.5 ul
716 Exonuclease I (ThermoFisher) for 30 minutes at 37°C and inactivated at 75°C for 15 minutes.
717 Sanger sequencing for each purified sample was performed using each 3' primer from the previous
718 BCR PCR amplification. Sequences were trimmed at Q30 using Geneious and submitted to
719 IMGT/HighV-QUEST for alignment (Alamyar et al, 2012). Primers were designed using 5' and
720 3' cDNA sequence for In-Fusion Cloning Kit and performed according to manufacturer's
721 instructions. If a 5' or 3' sequence was missing, then the closest matching IMGT germline
722 sequence was used for primer design. Heavy chains were inserted into IgG1 vectors, kappa and
723 lambda chains were cloned into vectors with their respective constant regions(Smith et al. 2009).
724 Cloned plasmids were sequenced and screened by ensuring sequences of chains matched original
725 cDNA sequence.

726

727 *Expression and purification*

728 For small scale transfections, 12 well plates of 293T cells at 80% confluence were transiently
729 transfected with 0.5ug each of heavy and light chain vectors using polyethylenimine (PEI). After
730 16 hours, media was removed and replaced with serum-free media. After 3-4 days, supernatants
731 were harvested and cell debris was removed by centrifugation at max speed in a microcentrifuge

732 for 1 minute. For large scale transfections, expression vectors containing paired heavy and light
733 chains were transiently transfected into 293T cells using polyethylenimine (PEI). Expression of
734 recombinant full-length human IgG monoclonal antibodies were carried out in serum-free basal
735 medium (Nutridoma-SP, Sigma-Aldrich). Four days after transfection, cell culture medium was
736 collected and protein was purified using HiTrapTM Protein G HP column (1ml, GE Healthcare).
737 Final IgG proteins were concentrated and buffer exchanged into 1x PBS using Millipore
738 concentrator (30K MWCO). IgG protein concentration is determined by Nanodrop 2000
739 spectrophotometer.

740

741 **Statistics**

742 Statistics used are described in figure legends and were determined using Prism (Graphpad). All
743 measurements within a group in a panel are from distinct samples except technical replicates used
744 in ELISAs as described. Statistical significance of all pairwise comparisons was assessed by two-
745 tailed nonparametric tests; Mann-Whitney for unpaired data and Wilcoxon signed rank tests for
746 paired data unless otherwise noted. No multiple hypothesis testing was applied and exact p-values
747 are displayed.

748

749 **Data Availability:**

750 All data generated or analysed during this study are included in this published article (and its
751 supplementary information files) or available from the corresponding author upon reasonable
752 request with the exception of a few blood draw samples that were used up in this study.

753

754 **Acknowledgements:**

755 We thank David M. Koelle for PBMC samples used for reagent testing, Florian Krammer for
756 vectors used to express the SARS-CoV-2 S RBD, Wesley C. Van Voorhis for historical negative
757 serum samples, Ben Murrell and the CoroNAb consortium for providing the Ty1 antibody, Ali
758 Ellebedy for providing the BO4 and CO2 antibodies, Mike Murphy and Deleah Pettie for
759 assistance with protein production, the Benaroya Research Institute biorepository for historical
760 negative PBMC samples, Noah Simon for assistance with statistical analyses, Makala Hale for
761 help with BCR sequencing, Brian Hondowicz for technical help, the Pepper, Gale, Campbell,
762 Rawlings and Hammerman labs for helpful discussion and the study volunteers for their
763 participation. This work was supported by the following funding: L.B.R and L.S (NIH2T32
764 AI106677), D.J.C. and P.M. (NIH R01AI127726, NIH U19AI125378-S1), J.A.H. (NIH
765 R01AI150178-01S1), H.R.W. (NIH TL1 TR002318), D.R. (SCRI, Research Integration Hub
766 Covid-19 Award), M.P. (NIH U01AI142001-02S1; R01AI118803); a Bill & Melinda Gates
767 Foundation grant to N.P.K. (OPP1156262); BWF #1018486 and COVID Pilot grant to M.P.;;
768 Emergent Ventures Fast Grant to M.P.

769

770 **Author contributions:**

771 M.P., L.B.R. and J.N. conceived the study. K.K.T. assisted in cohort recruitment and visit
772 scheduling. J.R., C.S., E.A.H., L.B.R, J.N. and K.K.T. processed and preserved blood and serum
773 samples. J.N., L.C., and N.P.K. generated proteins and L.B.R. generated and validated tetramer
774 reagents. L.S., J.N. and L.B.R performed ELISAs and L.S. and J.N performed sVNT assays. L.S.
775 analyzed serum data. H.R.W. and J.H. conceived, performed and analyzed innate cell phenotyping
776 experiments. L.B.R. and J.N. performed and analyzed antigen-specific B cell flow cytometry and
777 sorting. K.B.P. and P.M. conceived, performed and analyzed T cell experiments. C.T. sequenced

778 and generated mAb plasmids. Y.C. expressed and purified mAbs. J.E. and E.A.H. performed PRNT
779 assays. L.B.R., J.N., L.S., K.B.P., P.M. and M.P. drafted the manuscript. All authors helped edit
780 the manuscript. M.P. secured funds and supervised the project.

781

782 **Competing Interests:**

783 M.P., D.R., J.N., C.T., Y.C. and L.B.R. have filed a patent under the provisional serial no.
784 63/063,841. Other authors declare no competing interests.

785

786 **Additional Information**

787

788 **Correspondence and requests for materials** should be addressed to M.P.

789 **Supplementary Information** is available for this paper.

790 **Extended Data Figure/Table Legends:**

791

792 **Extended Data Table 1. Study cohort characteristics.**

793

794 **Extended Data Figure 1. Healthy controls do not have SARS-CoV-2 RBD or spike-specific**
795 **antibodies.**

796 ELISA dilution curves and AUC for anti-RBD **a)** and anti-spike **b)** IgG (left) and IgM (right) in
797 plasma collected prior to the SARS-CoV-2 pandemic (historical negatives, HN, black), during the
798 pandemic (healthy controls, HC, red, at Visit 2), and from individuals previously found PCR
799 positive for SARS-CoV-2 (CoV2⁺, blue, at Visit 1). Dashed line indicates mean + 3 SD of HN
800 AUC values. Statistical significance determined by two-tailed Mann-Whitney tests. Error bars
801 represent mean and SD (HN n=5, HC n=14, IgG CoV2⁺ n=1, IgM CoV2⁺ n=1).

802

803 **Extended Data Figure 2. PBMC innate populations in CoV2⁺ and HC individuals are not**
804 **different at Visit 1.**

805 **a)** Flow cytometry gating for CD15⁻CD3⁻CD19⁻CD56⁻HLADR⁺CD14⁺ monocytes (purple gate),
806 which were further divided into CD14^{lo}CD16⁺ (red gate), CD14⁺CD16⁺ (blue gate), and
807 CD14⁺CD16⁻ monocytes (green gate), and CD15⁻CD3⁻CD19⁻CD56⁻CD14⁻CD304⁺CD123⁺
808 plasmacytoid dendritic cells (pDCs) (pink gate). **b)** Percent monocytes and **c)** pDCs of live PBMCs
809 and **d-f)** percent monocyte subsets of monocytes in PBMCs from healthy controls (HC) and
810 previously SARS-CoV-2 infected (CoV2⁺) individuals. Statistical significance determined by two-
811 tailed Mann-Whitney tests. Error bars represent mean and SD (HC n=15, CoV2⁺ n=14, 2
812 experiments).

813

814 **Extended Data Figure 3. Bulk PBMC T Cells return to immune quiescence by Visit 1.**

815 **a)** Representative flow cytometry plots and **b)** frequencies of $\alpha\beta$ and $\gamma\delta$ T cell subsets at Visit 1
816 (V1) in PBMCs from historical negative (HN), healthy control (HC) and SARS-CoV-2-recovered
817 (CoV2⁺) PBMCs. **c)** Representative flow cytometry plots and **d)** frequencies of CD4⁺ and CD8⁺ T
818 Cell effector/activation states of total non-naive, memory CD4⁺ or CD8⁺ T Cells
819 (CD45RA⁺CCR7^{+/-}) at V1 in HC and CoV2⁺ PBMCs. **e)** Representative flow cytometry plots and
820 **f)** frequencies of CD4⁺ memory and T-helper subsets at V1 in HN/HC and CoV2⁺ PBMCs. **g)**
821 Representative flow cytometry plots and **h)** frequencies of cTfh (CXCR5⁺CD45RA⁻) and cTfh
822 activation (ICOS⁺PD-1⁺) and helper (CXCR3^{+/-}CCR6^{+/-}) subsets at V1 in HC and CoV2⁺ PBMCs.
823 Statistical significance determined by two-tailed Mann-Whitney tests. Error bars represent mean
824 and SD (HN n=6, HC n=15, CoV2⁺ n=14, 2 experiments).

825

826 **Extended Data Figure 4. PBMC B Cell and antibody response at two memory time points.**

827 **a)** Frequency of plasmablasts (PBs, CD20⁻CD38^{hi}) of live, CD3⁻CD14⁻CD16⁻ PBMCs and **b)**
828 cycling cells (Ki67⁺) and **c)** T-bet⁺ cells of live, CD3⁻CD14⁻CD16⁻CD20⁺ PBMCs from healthy
829 control (HC) and SARS-CoV-2-recovered (CoV2⁺) individuals at Visit 1 (V1) and Visit 2 (V2)
830 (HN n=14, V1 HC n=15, V2 HC n=14 (PB) n=15 (Ki67, T-bet) , V1 CoV2⁺ n=14, V2 CoV2⁺
831 n=14, 2 experiments). **d)** ELISA dilution curves and AUC for anti-spike IgG (left), IgM (center),
832 and IgA (right) from HC and CoV2⁺ plasma at V1. Dashed line indicates 3 mean + 3 SD of the
833 HC AUC values. Each symbol is a different individual and is consistent in d), f) and h) (HC n=15,
834 CoV2⁺ n=15). **e)** Spearman correlation of V1 anti-RBD and anti-spike IgG (left), IgM (center),
835 and IgA (right) AUC (HC n=15, CoV2⁺ n=15). **f)** V2 HC AUC values and **g)** RBD inhibition at

836 1:10 plasma dilution were normalized to V1 CoV2⁺ samples run with V2 samples and value for
837 each HC individual from V1 and V2 are paired (V1 HC n=12, V2 HC n=12). **h)** Percent
838 neutralization dilutions curves determined by PRNT for CoV2⁺ and HC samples (V1 HC n=2, V1
839 CoV2⁺ n=15, V2 HC n=2, V2 CoV2⁺ n=14). Statistical significance for unpaired data determined
840 by two-tailed Mann-Whitney tests and, for paired data, by two-tailed Wilcoxon signed-rank tests.
841 Error bars represent mean and SD.

842

843 **Extended Data Figure 5. Detecting SARS-CoV-2 RBD-specific B cells in PBMCs.**

844 **a,b)** SARS-CoV-2 RBD tetramer detected increased numbers of RBD-specific B cells (Live, CD4⁺
845 CD8⁻B220⁺ and CD138⁺B220⁻RBD tetramer⁺Decoy⁻) which had increased frequencies of germinal
846 center B cells (GCB, GL7⁺CD138⁻) and plasmablasts (PB, CD138⁺GL7⁻) in popliteal lymph nodes
847 from mice 7-10 days post-immunization with RBD/CFA compared naive (n=3 mice/treatment in
848 3 experiments). **c)** Representative flow cytometry gates for phenotyping in Figure 2 set on total B
849 cells from healthy controls (HC) and SARS-CoV-2-recovered (CoV2⁺) in two panels (surface, top;
850 intracellular, bottom). **d)** Left, frequencies of RBD-specific B cells with naive (CD21⁺CD27⁻) and
851 memory (CD21⁺CD27⁺/CD21⁻CD27⁺/CD21⁻CD27⁻) phenotypes from HC and CoV2⁺ PBMCs at
852 Visit 1 (V1) and Visit 2 (V2). Right, frequency of MBCs (populations outlined in red). **e)** Number
853 of cycling (Ki67⁺) RBD-specific MBCs (HN n=14, V1 HC n=12, V2 HC n=13, V1 CoV2⁺ n=15,
854 V2 CoV2⁺ n=14). Frequency of RBD-specific MBCs expressing **f)** indicated BCR isotype (HN
855 n=14, V1 HC n=12, V2 HC n=13, V1 CoV2⁺ n=15, V2 CoV2⁺ n=14) or **g)** T-bet. Number of **h)**
856 resting (T-bet^{lo}) and **i)** recently activated (T-bet^{hi}) RBD-specific MBCs. Statistical significance for
857 unpaired data determined by two-tailed Mann-Whitney tests and, for paired data, by two-tailed

858 Wilcoxon signed-rank tests. Error bars represent mean and SD (HN n=14, V1 HC n=15, V2 HC
859 n=15, V1 CoV2⁺ n=15, V2 CoV2⁺ n=14, unless otherwise noted, 2 experiments).

860

861 **Extended Data Figure 6. Bulk CD4 and CD8⁺ T cell cytokines expression.**

862 **a)** Representative cytokine gating on CD69⁺ICOS⁺ CD4⁺ T Cells from PMA/Ionomycin -activated
863 CD4⁺ cTfh (CXCR5⁺) and non-cTfh (CXCR5⁻) T Cells. **b)** Sorting strategy and **c)** frequency of
864 proliferated (CXCR3⁺CPD^{lo}) naive, T central memory (T_{CM}), and T effector memory (T_{EM}) cells
865 from HC and CoV2⁺ PBMCs at Visit 1 and Visit 2 after 5-6 days of culture with autologous
866 monocytes and SARS-CoV-2 spike protein or vehicle (V1 HC n=3, V2 HC n=4, V1 CoV2⁺ n=3,
867 V2 CoV2⁺ n=4). **d)** Representative flow cytometry plots of cytokine expression from
868 PMA/Ionomycin-activated CD8⁺ T cells (HN n=6, HC n=15, CoV2⁺ n=14). Statistical significance
869 for unpaired data determined by two-tailed Mann-Whitney tests and, for paired data, by two-tailed
870 Wilcoxon signed-rank tests. Error bars represent mean and SD (2 experiments).

871

872 **Extended Data Figure 7. Generation of neutralizing antibodies by RBD-specific MBCs.**

873 **a)** Gating strategy for sorting RBD-specific B cells. **b)** IgG ELISA to confirm expression of
874 antibodies in transfected cell culture supernatants. **c)** RBD ELISA of purified monoclonal
875 antibodies. Negative control is an irrelevant *Plasmodium*-specific antibody.

876

877 **Extended Data Table 2. RBD-specific MBC-derived antibody amino acid sequences.**

Extended Data Table 1: Study cohort characteristics

	Previously SARS-CoV-2 Infected (CoV2⁺)	Healthy Controls (HC)	Historical Negatives (HN)
Number of participants ¹	15	17	14
Age (years)	47 (28 – 71)	42 (24 – 57)	47.5 (27 – 72)
Sex	27% Male, 73% Female	47% Male, 53% Female	21% Male, 79% Female
Number of symptoms ^{2,3}	5 (1 – 7)	NA	ND
Symptom duration (days)	13 (2 – 31)	NA	ND
Time from symptom onset to Visit 1 (days)	35.5 (19 – 44)	NA	NA
Time from symptom onset to Visit 2 (days)	86 (73 – 110)	NA	NA
Time from SARS-CoV-2 positive PCR test to Visit 1 (days)	28 (20 – 35)	NA	NA
Time from SARS-CoV-2 positive PCR test to Visit 2 (days)	77.5 (64 – 97)	NA	NA
Time from Visit 1 to Visit 2 (days)	46 (39 – 69)	47 (40 – 61)	NA
Year samples drawn	2020	2020	2016 – 2019

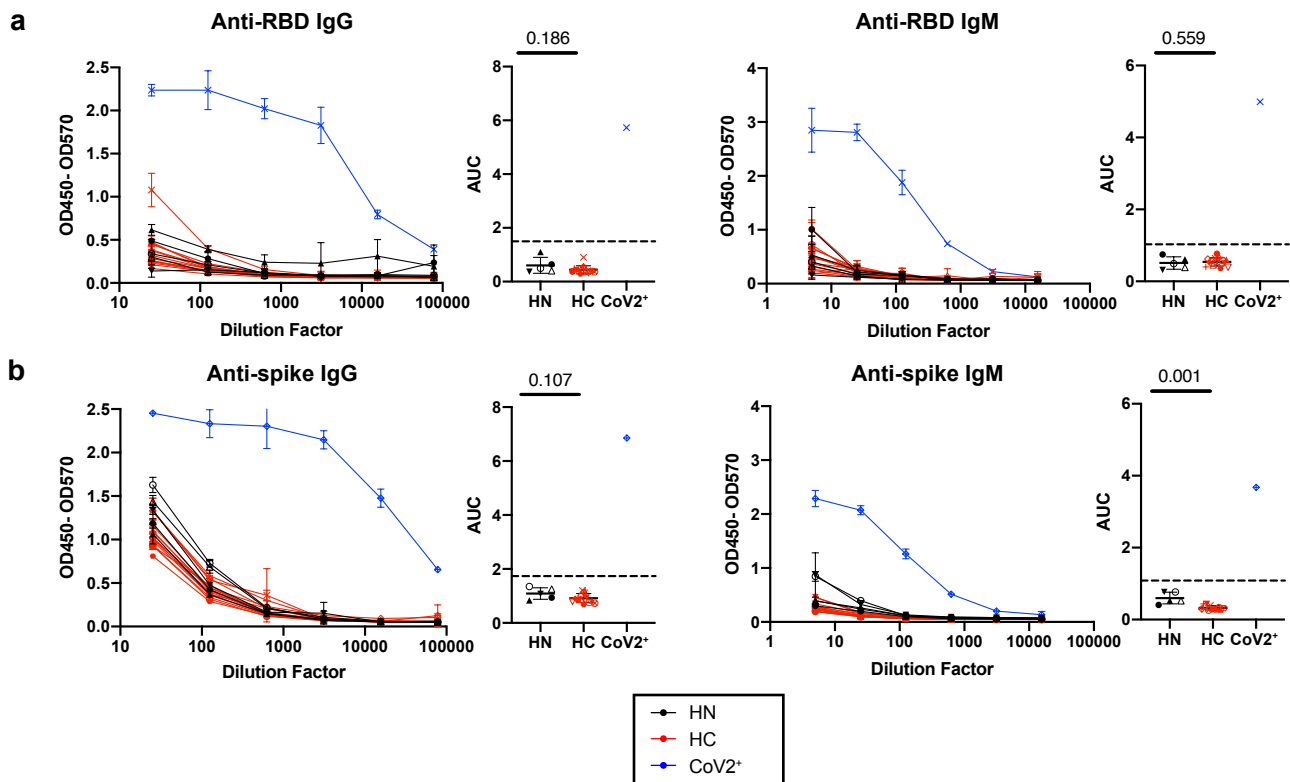
¹ Blood drawn from 14 CoV2⁺ and 13 HC at Visit 1 and Visit 2. 1 CoV2⁺ and 2 HC were only drawn with Visit 1. 2 HC were only drawn with Visit 2.

² All CoV2⁺ individuals reported symptoms. 9 HCs reported symptoms and 2 HC had negative SARSCoV-2 PCR results.

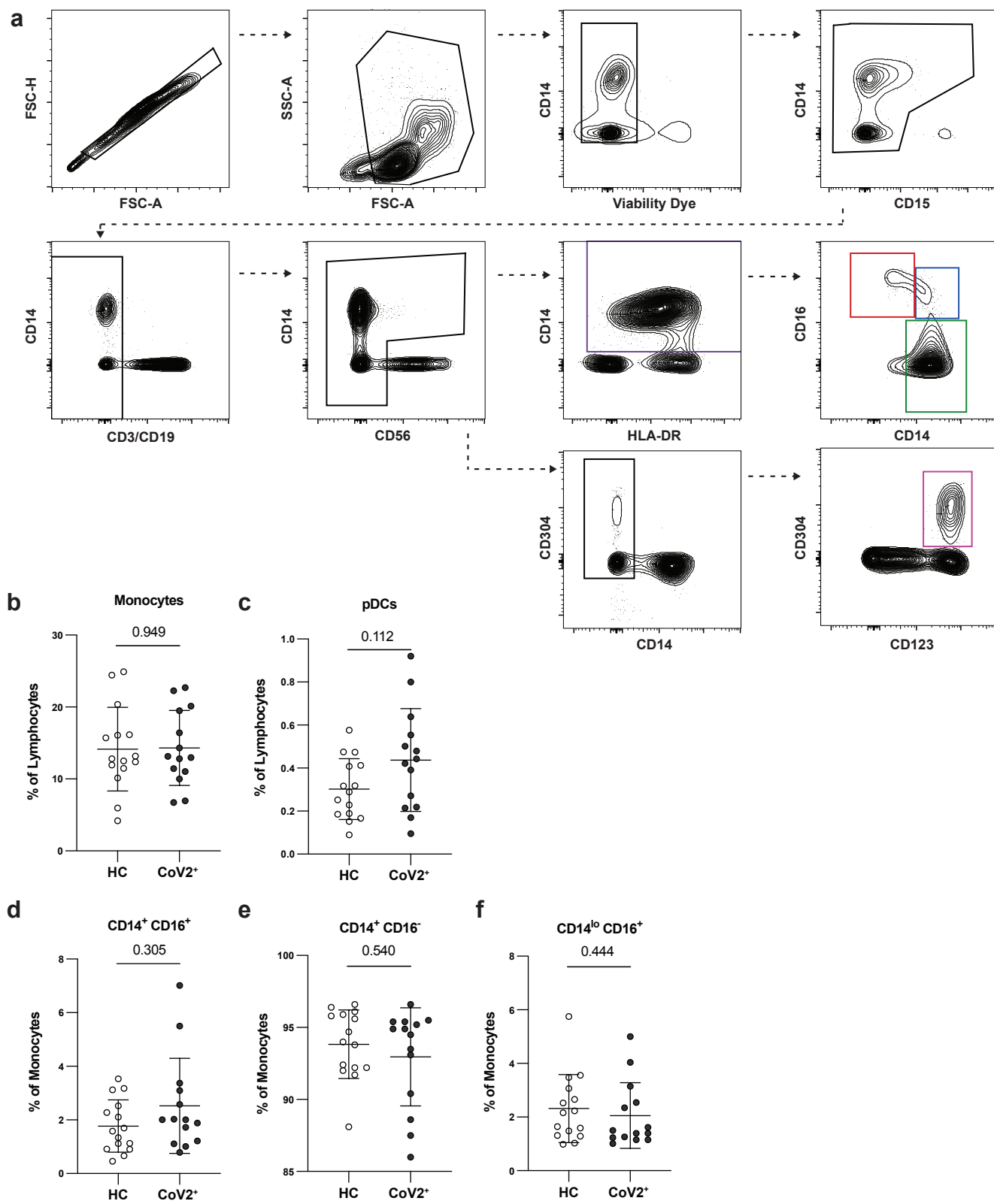
³ The symptoms surveyed were fever, chills, cough, runny nose, fatigue, muscle ache and difficulty breathing.

Previously SARS-CoV-2 infected (CoV2⁺) and healthy control (HC) volunteers were consented and enrolled for this study. Values are reported as the median with the range in parentheses. ND = No data, NA = Not applicable.

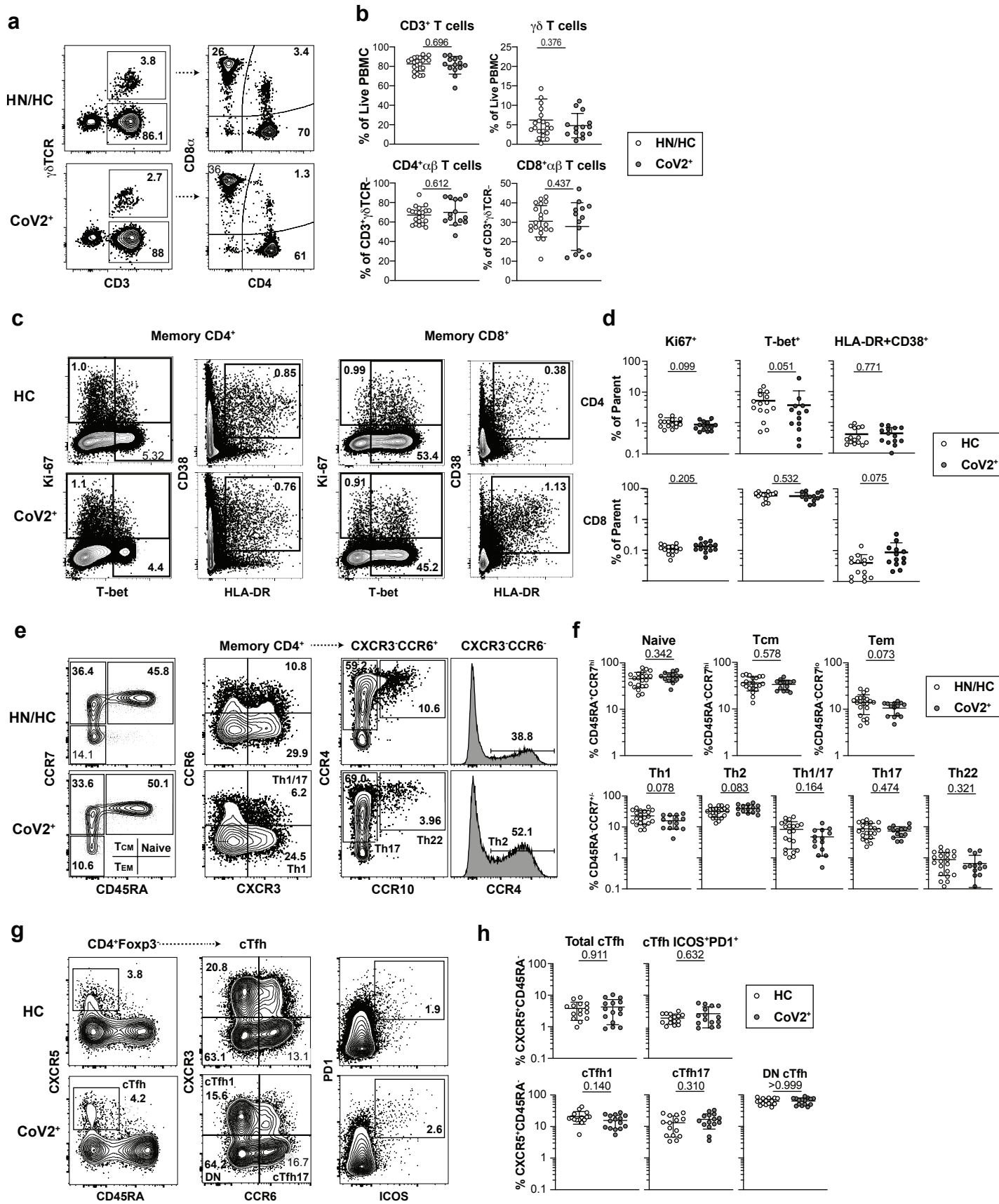
Extended Data Figure 1



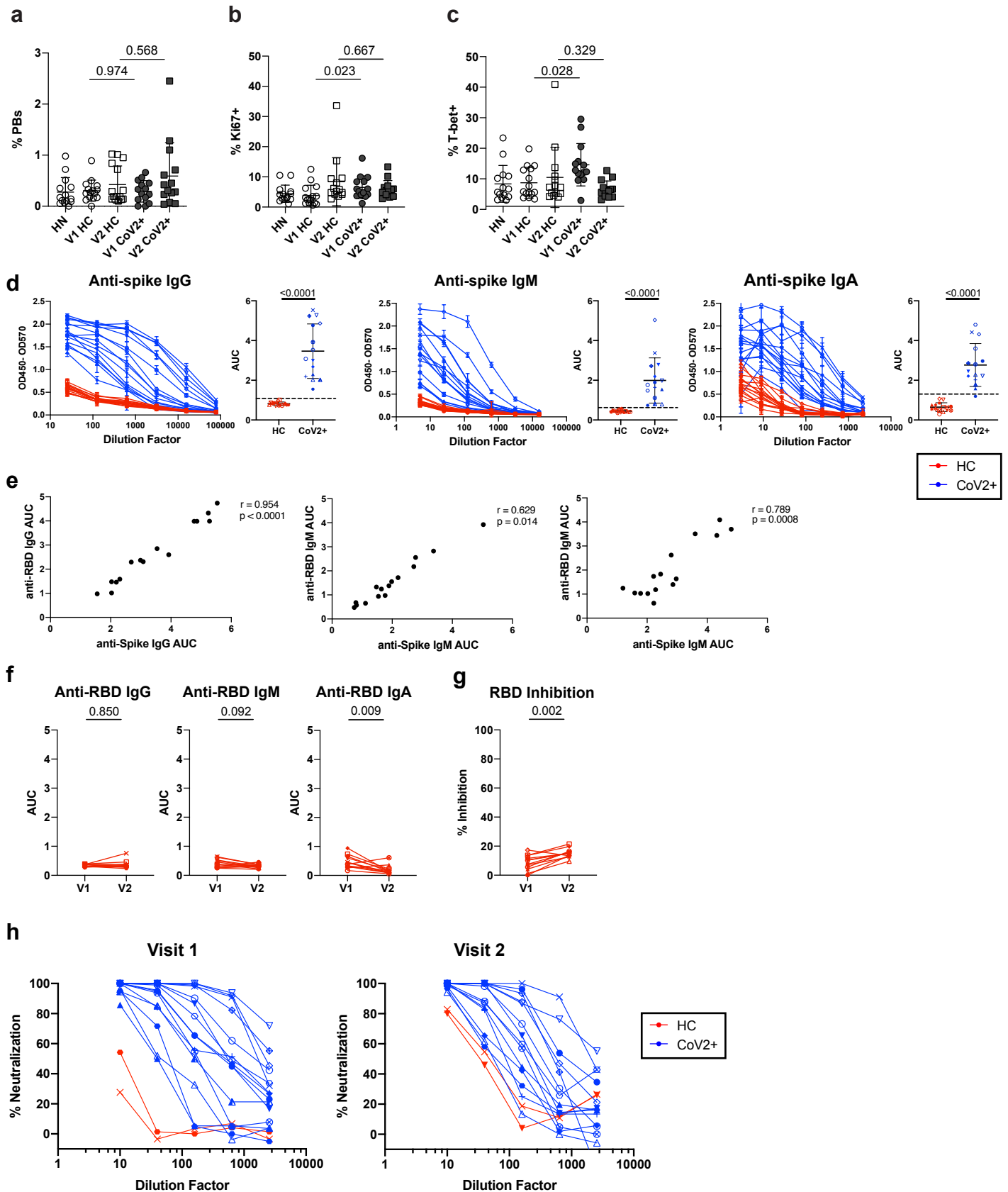
Extended Data Figure 2



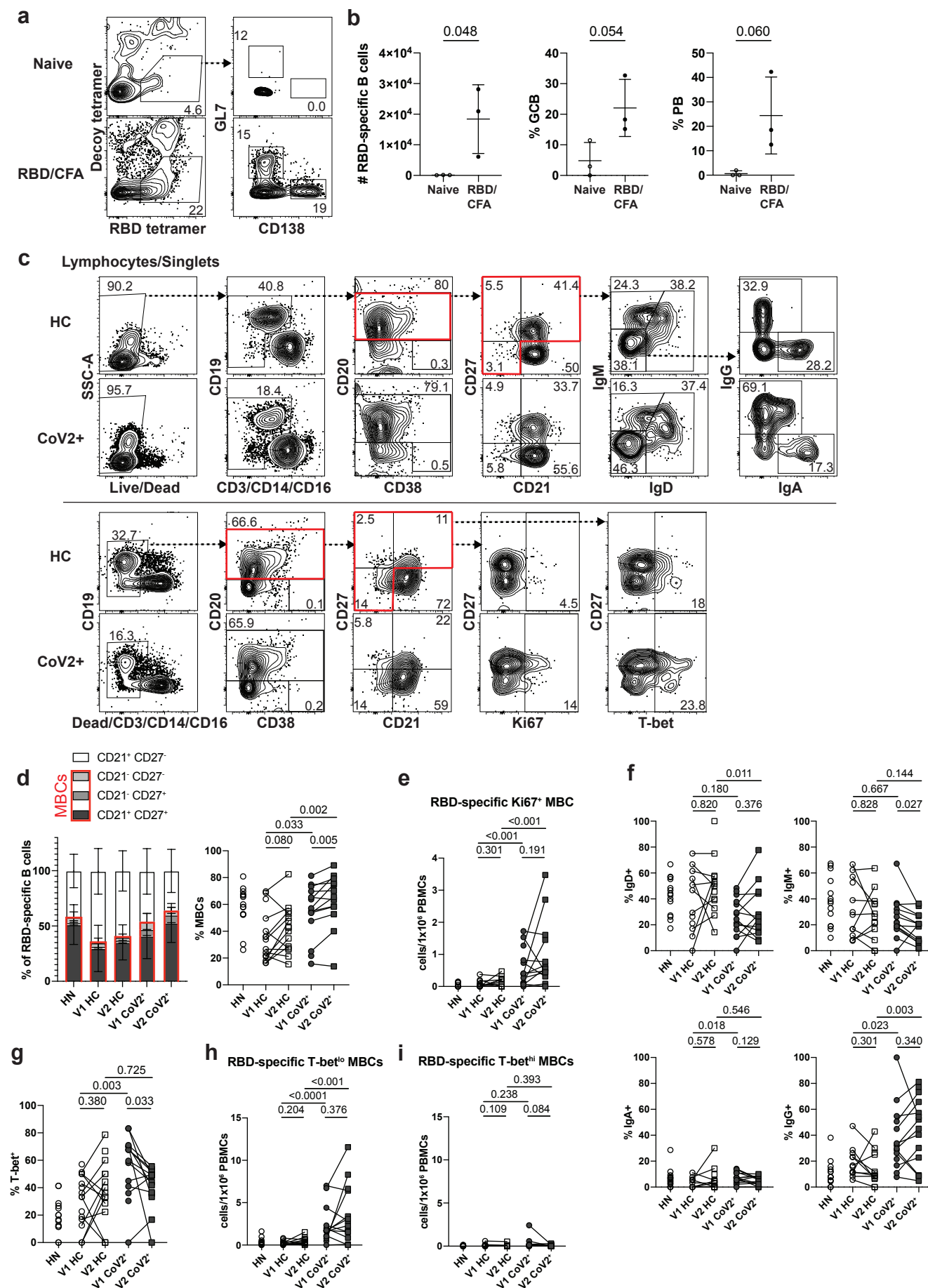
Extended Data Figure 3



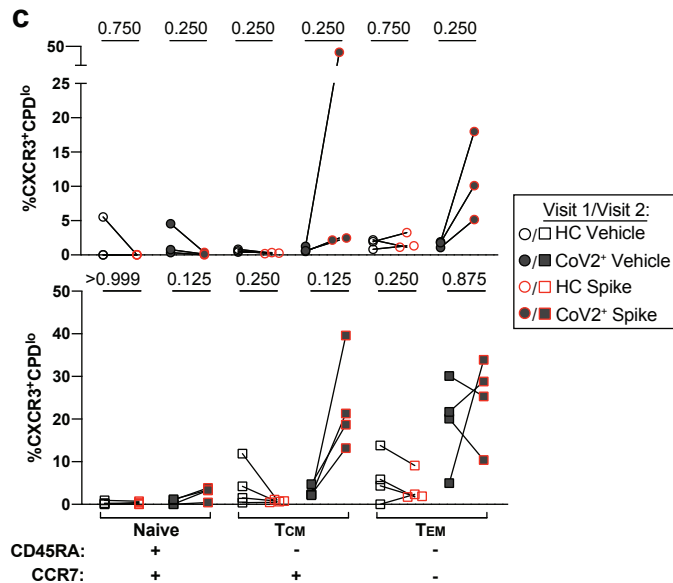
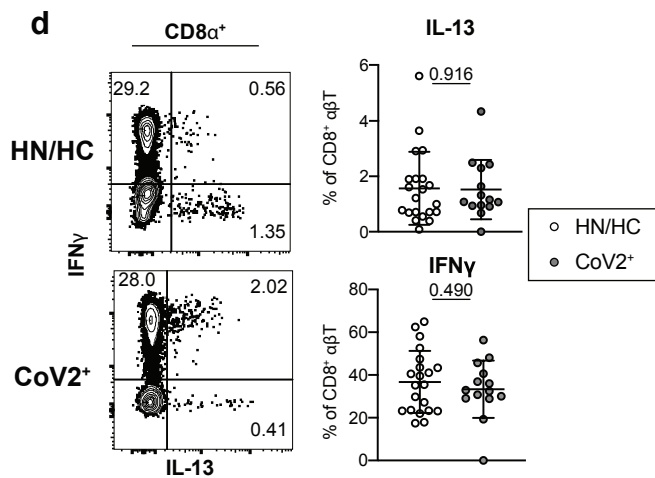
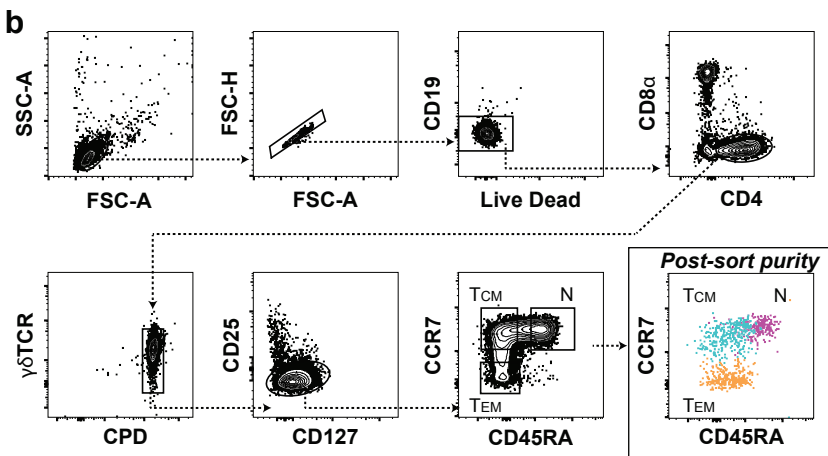
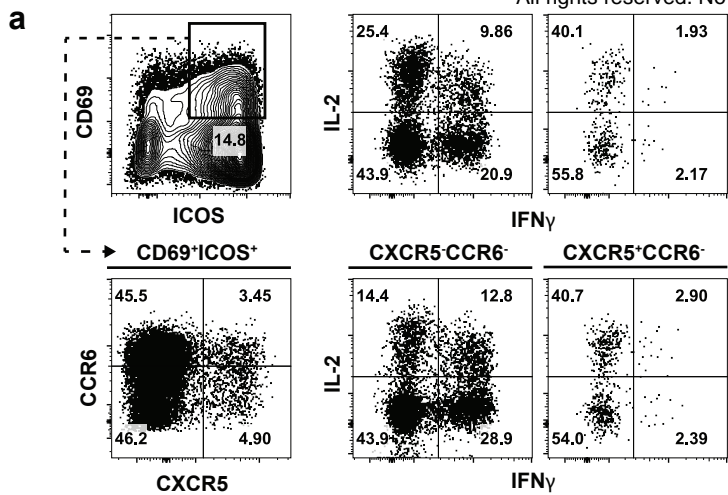
Extended Data Figure 4



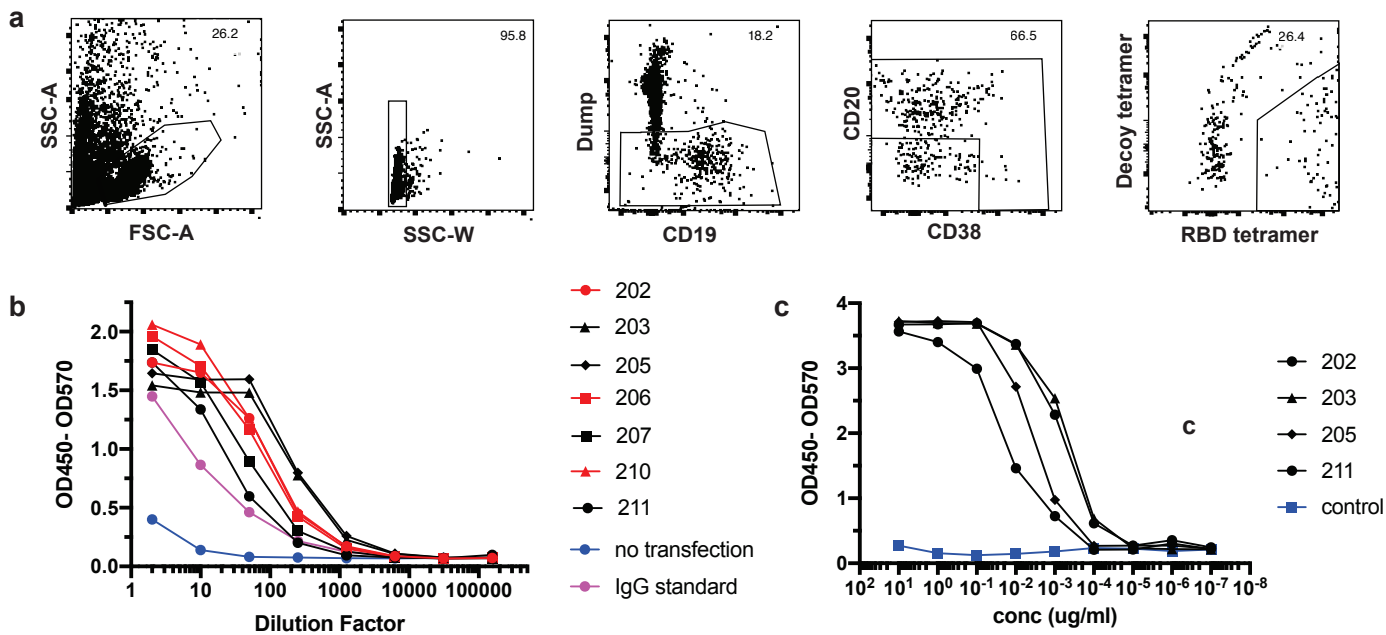
Extended Data Figure 5



Extended Data Figure 6



Extended Data Figure 7



Extended Data Table 2.

mAb ID	Chain	AA Sequence
202	Heavy	EVQLVESGGGLVQPGGSLRLSCAASEITVSSNYMSWVRQAPGKGLEWWSLIYSGGS TFYADSVKGRFIISRDNKNTLYLQMNSLRAEDTAVYHCARGGEEPLPFDPWGQGLTV TVSS
202	Lambda	QSVLTQPPSVSGAPGQRVTISCTGSSSNIGAGYDVHWYQQLPGTAPKLLIYGNSNRP SGVPDRFSGSKSGTSASLAITGLQAEDEADYYCQSYDSSLVSVVFGGGTKLTVL
203	Heavy	QVQLVQSGAEVKKPGSSVKV/SCKASGGTFSSYPISWVRQAPGQGLEWMGRIIPILRV ANFAQRFEGRVITADKSTGTAYMELSSLRSEDTAMYCARDEAQTNTNWFDPWG QGLTVTVSS
203	Lambda	QSVLTQPPSVSGAPGQRVIISCTGSNSNIGAGYDVHWYQQLPGTAPKLLIYGNNRPS GVPDRFSGSKSGTSASLAITGLQAEEDGADYYCQSYDSSLSDVVFGGGTKLTVL
205	Heavy	QVQLQESGPGLVKPSSETLSLTCTVSGGSVSSGSYYWSWIRQPPGKGLEWIGYIYYSG STNYPNPSLKSRTISVDTSKNQFSLKLSVTAADTAVYYCARVPRFISDWYPFYSIDYW GQGTLTVTVSS
205	Lambda	QSALTQPPSASGSPGQSVTISCTGTSSDIGGYNVSWYQQHPGKAPKLMIEVSKRP SGVPDRFSGSKSGNTASLTVSGLQAEDEADYYCSSYAGSTVLFGGGTKLTVL
206	Heavy	EVQLVESGGGLVQPGGSLRLSCAVSGFTVSSNYMSWVRQAPGKGLEWWSVIYTG GTYADSVKGRFTISRDNKNTLYLQMNTLRAEDTTVYYCARGDGSYYRAFDYWGQ TLTVTVSS
206	Kappa	DIQMTQSPSSLSASVGDRTITCRASQSSISNYLNWYHQKPGKAPKLLIYAASSLQSGV PSRFSGSGSGTDFTLTISSLQPEDFATYYCQQSYSPPTFGPGTKVEIK
207	Heavy	EVQLVESGGGLVQPGGSLRLSCAASGFTFSSYAMSWVRQAPGKGLEWWSAISGSGD STYHADSVKGRFTISRDNKNTLYLQMNSLRAEDTAVYYCAKDPGTVTTYEYFQHWG QGLTVTVSS
207	Lambda	SYVLTQPPSVSVAPGKTARITCGGNNIGSKSVHWYQQRPGHAPVLVIYYDSDRPSGIP ERFSGNSGNTATLTISRVEAGDEADYYCQVWDGSSDHPGMVFGGGTKLTVL
210	Heavy	EVQLVESGGGLIQPGGSLRLSCAASGFTVSRNYMNWVRQAPGKGLEWWSVIYSGGS TFYADSVKGRFTISRDNKNTLYLQMNSLRAEDTAVYYCARDASSYIDWGQGLTVTV SS
210	Kappa	DIQMTQSPSSLSASVGDRTITCRASQSISSYLNWYQQKPGKAPKLLIYASSSLQRGV PSRFSGSGSGTDFTLTISSLQPEDFATYYCQQSYSTPITFGQGRLEIK
211	Heavy	QVQLQESGPGLVKPSSETLSLTCTVSGGSISSYYWSWIRQPPGKGLEWIGYIYYS GSTNYPNPSLKSRTISVDTSKNQFSLKLSVTAADTAVYYCAGDFWSPDPSYYYGMDVW GQGTTVTVSS
211	Kappa	DIQMTQSPSSVSASVGDRTITCRASQGISSWLAWYQQKPGKAPKLLIYAASLQSGV PSRFSGSGSGTDFTLTISSLQPEDFATYYCQQANSFPRTFGQGRLEIK

Extended Data Table 2. Amino acid sequence of monoclonal antibody variable regions.